ICARUS 36, 1–50 (1978)

Cloud Microphysics: Analysis of the Clouds of Earth, Venus, Mars, and Jupiter

WILLIAM B. ROSSOW[1]

Geophysical Fluid Dynamics Program, Princeton University, Princeton, New Jersey 08540

Received May 31, 1977; revised April 3, 1978

A simple method of deducing the probable microphysics of a cloud is developed that uses only information about cloud particle mean size, composition, number density, and atmospheric structure. This analysis is applied to the sulfuric acid clouds of Venus, the water ice and dust clouds of Mars, and the ammonia–water and ammonia ice clouds of Jupiter. The Venus cloud layer most closely resembles smog and haze layers on Earth with no sharp concentration gradients. The cloud microphysics is dominated by coagulation, sedimentation, and turbulent mixing. No precipitation is formed. The water ice clouds on Mars resemble tenuous, non-precipitating cirrus clouds on Earth. Deposition of condensed water on Mars only occurs from surface fogs or direct condensation on the surface. These fogs can provide a very efficient dust deposition mechanism. The observed settling behavior of the great dust storm of 1971 suggests sedimentation at the surface from a turbulent cloud with coagulation growth of large particles to replace those lost by sedimentation, analogous to the nighttime evolution of submicron tropospheric aerosols on Earth. The ammonia–water and ammonia ice clouds on Jupiter produce precipitation on time scales $<10^4$ sec. The vertical structure of all clouds is significantly altered. The activity of the lower ammonia–water cloud has significant effects on the vertical distribution of other gases and aerosols, on the vertical transport of heat, and on the dynamics in this portion of the atmosphere.

I. INTRODUCTION

All planetary atmospheres contain large numbers of suspended particles referred to as aerosols or clouds. Even though these particles are only a negligible fraction of the mass of an atmosphere, they can have a significant effect on the radiative energy transfer. Further, since the atmospheric motions driven by the radiation control the distribution of these particles, strong nonlinear coupling can occur between the radiation and the motions. The paucity of observations of other atmospheres, especially of the aerosols in them, together with the primitive state of the theory of atmospheric dynamics, has limited simulations of these atmospheres to very simple models which usually neglect aerosol effects altogether. Further progress will require that these effects be incorporated into the models. One preliminary step towards understanding the role played by aerosols in other atmospheres is finding an analogous aerosol or cloud from among the more familiar examples on Earth. To that end, I present a brief discussion of cloud physics theory with a description of clouds on Earth and a discussion of its application to clouds on Venus, Mars, and Jupiter.

The study of aerosols involves so many disciplines, each with its own vast literature, that it is difficult to find a single

[1] Work begun while author was at the Laboratory for Planetary Studies, Cornell University.

0019-1035/78/0361-0001$02.00/0

comprehensive treatment of the subject.[2] Moreover, the applicability of the theory to other planetary aerosols has not been thoroughly discussed. The first purpose of the next four sections is to distill and collect material to serve as an introduction and guide to this broad and ill-defined subject. This discussion is not intended to be encyclopedic. Instead I have limited the physical processes considered to the most important ones for most aerosols. I have neglected many other processes because either the theory or the corroborating data, or both, are lacking. In many cases, the simplification of quite detailed theories is necessitated by a lack of an equivalent amount of detail in the observations of aerosols on other planets or even on Earth. The second purpose of these four sections is to describe the important aerosol processes in sufficient detail to point out the limitations of the theory and the simplifications required by the available data. These sections set the stage for the analogies in the final sections between the clouds on Earth and those on other planets.

The shortage of observational detail is a familiar and frustrating characteristic of the study of planetary atmospheres and of aerosols in particular. For instance, in the atmosphere of the outer planets, even the cloud composition is uncertain. In this situation the only questions which can be addressed are the very basic ones about the mean atmospheric structure and the predominant processes at work. Generally, only qualitative arguments are possible. Two such arguments are based on the comparison of the characteristic time constants of processes to determine their relative importance and on analogies with better understood and observed systems on Earth. I use both of these approaches here in an analysis with three steps.

(i) The discussion of processes in Sections II to V culminates in approximate formulas for their time constants which are compared as functions of the mean particle radius in a constant mass cloud.

(ii) The comparison method is tested on Earth aerosols in Section VI to define the basic models to be used in the analogies with other aerosols. The limitations of this method are also discussed.

(iii) The proper analogies between aerosols on Earth and on other planets are then more firmly established in Section VII by applying the same comparison of time constants in these other aerosols. The conclusions are listed in Section VIII.

II. USEFUL DEFINITIONS AND CONCEPTS

Since I draw material from many different disciplines related by their common study of aerosols, but divided by their different jargons, I present in this section brief definitions of the important terms and discussion of the central concepts used throughout this paper. There are five major aerosol processes.

(*a*) *Condensation–evaporation* (Section III). These terms refer, here, to the conversion of vapor to particles and the reverse regardless of whether the condensed phase is liquid or solid. The distinction between a large molecule and a small particle is not precise, but the smallest group of molecules that retains some particle-like properties has a radius $\sim 10^{-7}$ cm. [See the discussion in Section III, Part A, Section V, Part A, and Twomey (1977).] All solid phase aerosols are called snow or ice without consideration of composition. Precipitation is formation of cloud particles for which the evaporation time is much longer than the sedimentation time. For convenience, I define the saturation, S, as the ratio of two vapor densities rather than the

[2] There are several excellent books which, taken together, form a nearly complete treatment of aerosols. These books are marked by asterisks in the reference list. The recent book by Twomey (1977) deserves special mention.

vapor pressures. The supersaturation is $s = S - 1$. The thermodynamic saturation, S_∞, or supersaturation, s_∞, involves the equilibrium vapor density of the pure vapor over a flat surface of pure condensate. In general, the effective value of s for condensation growth differs from s_∞. Evaporation occurs when $s < 0$. These processes play a primary role in the creation, growth, and destruction of planetary aerosols.

(*b*) *Sedimentation* (Section IV, Part A). This term refers to the falling of aerosols under the influence of gravity onto a planetary surface or into a higher temperature, evaporation region. This process is a primary sink for all planetary aerosols.

(*c*) *Wind transport–surface interactions* (Section IV, Part B). The first term refers to the vertical and horizontal transport of aerosols by large-scale atmospheric motions, considered as steady winds, and small-scale, turbulent motions. Wind transport can act as either a source or sink of particles for a particular region of the atmosphere. The second term refers to the interaction between aerosols on or near planetary surfaces and the turbulent surface winds. This interaction can either deposit aerosols on the surface or raise them from it. The latter process is a primary source of aerosols in terrestrial planetary atmospheres.

(*d*) *Coagulation* (Section V, Part B). This term refers to the formation of a single particle from two colliding particles. There are also several other words, used interchangeably in the literature, that have the same meaning. For convenience, I use the word coagulation to refer only to collisions caused by the Brownian motion of aerosols. This is one of the two major collisional processes in planetary aerosols.

(*e*) *Coalescence* (Section V, Part C). I use this word to refer only to collisions caused by the different sedimentation velocities of different size aerosols, the other major collisional process. In water clouds on Earth, this process is often called the warm rain process.

The following symbols are used throughout this paper while others are defined as needed.

- a Particle radius
- g Acceleration of gravity
- k Boltzmann's constant
- m Mass of atmospheric gas molecule
- m_v Mass of vapor molecule
- s Sticking efficiency
- t Time
- u Wind velocity
- v Particle velocity
- A Ratio of particle radii such that $A \leqslant 1$
- D Classical diffusion coefficient
- L Latent heat of vaporization
- M Particle mass $= 4\pi\rho_p a^3/3$
- N Total particle number density $= \int_0^\infty n(M, t)dM$
- R Universal gas constant
- T Absolute temperature
- V Terminal velocity of particles
- α Molecular sticking efficiency, condensation coefficient
- α' Accommodation coefficient
- η Atmospheric dynamic viscosity
- λ Gas mean free path
- μ Mass of cloud per unit volume $= \int_0^\infty Mn(M, t)dM$
- ρ Atmospheric density
- ρ_p Particle density
- ρ_v Vapor density
- ρ_s Saturation vapor density
- σ Surface energy or tension
- τ Time constant

The investigation of the different planetary aerosols requires theories that apply

for atmospheric densities that vary over at least five orders of magnitude and for particle sizes that vary over more than six orders of magnitude. To help define the different physical regimes encountered, I use the following dimensionless numbers.

1. The value of the Knudsen number

$$\mathrm{Kn} \equiv \lambda/a, \tag{1}$$

determines whether the interaction of atmospheric gases with an aerosol particle is best described by the continuum mechanics of a fluid ($\mathrm{Kn} \ll 1$, classical regime) or by the statistical mechanics of a Maxwell–Boltzmann ensemble ($\mathrm{Kn} \gg 1$, gas kinetic regime). In the difficult transition regime ($\mathrm{Kn} \sim 1$), where neither of these theories is valid, a rigorous theory and confirming data are lacking. The theories for the other two regimes can be formally joined across the transition by use of the Cunningham correction factor, $(1 + \beta\mathrm{Kn})$, where β is the Cunningham "constant." Data for falling spheres (Berry and Pranger, 1974) and theoretical results for mass diffusion in this regime (Fuchs and Sutugin, 1970) show that β is a weak function of Kn. Since β only varies between ≈ 1.2 and ≈ 1.6, I use $\beta = \frac{4}{3}$ throughout.

2. In the classical regime, the atmosphere can be treated as an incompressible fluid as long as the particle motions are such that the Mach number

$$\mathrm{Ma} \equiv v/C_s \ll 1, \tag{2}$$

where C_s is the speed of sound. This condition is met for all aerosols considered here.

3. The nature of the gas flow past a moving particle is determined by the relative importance of the gas inertial and drag forces on the particle. The flow is dominated by viscous drag forces when the Reynolds number

$$\mathrm{Re} \equiv 2\rho a v/\eta, \tag{3}$$

is $\ll 1$ (Stokes regime) and by gas inertial forces when $\mathrm{Re} \gg 1$ (turbulent regime). The transition regime is discussed in Section IV, Part A.

4. For particle motions in accelerated gas flows, two regimes are defined by the Stokes number

$$\mathrm{Stk} \equiv d/a, \tag{4}$$

where the stopping distance, d, is the distance over which the particle's velocity is significantly altered by the gas drag. The motion of the particles follows the streamlines of the flow for $\mathrm{Stk} \ll 1$, but is unaffected by the flow for $\mathrm{Stk} \gg 1$. The value of Stk is discussed more fully in Section IV, Part B.

5. For liquid droplets moving through a gas, the hydrodynamic pressure of the flow produces significant distortion of the droplet when it exceeds the surface tension pressure, that is, when the Weber number

$$\mathrm{We} \equiv \rho a v^2/2\sigma > 1. \tag{5}$$

The relationships between the five major processes affecting aerosols and the aerosol properties are illustrated by the simple flow diagram in Fig. 1. The mass density of the particles is given by their number density and mean particle radius. There are three general types of aerosols or clouds.

(*i*) *Dust clouds.* This term refers to any cloud in which vapor processes are negligible and only particle processes are operative. In Fig. 1 the particle processes are represented by $\tau_{\mathrm{growth}}^{-1}$, the collisional growth rate (coagulation or coalescence), by $\tau_{\mathrm{supply}}^{-1}$, the rate at which winds raise dust from a surface and transport it into the cloud region, and by $\tau_{\mathrm{fall}}^{-1}$, the sedimentation rate. The process which controls the removal rate of particles, $\tau_{\mathrm{remove}}^{-1}$, depends on the nature of the winds and the surface under the cloud. A strong wind over a particle covered surface produces a net cloud growth, while the same wind over a particle free surface produces a net

cloud decay. In the latter case, $\tau_{\text{remove}}^{-1}$ by wind transport can be $> \tau_{\text{fall}}^{-1}$. The distinction between small and large particles is made by their sedimentation rate. For small particles, $\tau_{\text{supply}}^{-1}$ or $\tau_{\text{remove}}^{-1}$ by wind transport is $> \tau_{\text{fall}}^{-1}$ under ambient wind conditions, while for large particles, $\tau_{\text{fall}}^{-1} > \tau_{\text{supply}}^{-1}$ or $\tau_{\text{remove}}^{-1}$. Clearly, the definition changes with the winds. Although there are important surface processes which can inject large particles directly into the atmosphere, Fig. 1 shows only the production of large particles by collisional growth processes. Direct injection is important only very near the planetary surface.

(ii) Cooling clouds. This term refers to the type of condensate cloud which forms when a volume of gas is cooled, either dynamically or radiatively, reducing ρ_s below ρ'_v, at a rate τ_*^{-1} in Fig. 1. The subsequent condensation consumes the vapor in excess of ρ_s, represented by ρ_v. The total mass density, $\rho'_v = \rho_s + \mu$, remains constant until particle removal processes become important. Since the location of such a cloud is a sensitive function of temperature, it is generally surrounded by cloud free gas so that $\tau_{\text{supply}}^{-1}$ does not apply. In general, the time required to attain a balance between vapor supply and vapor consumption by condensation, viz., $\tau_*^{-1} = \tau_{\text{cond}}^{-1}$, is very short compared to all other time constants in a cooling cloud. The particle size attained is limited either by the removal of the vapor supply on a dynamic time scale or by the lifetime of the particles in the cloud, i.e., $\tau_{\text{cond}}^{-1} = \tau_{\text{remove}}^{-1}$. A nonprecipitating cloud (no large particles or precipitation in Fig. 1) forms when $\tau_{\text{remove}}^{-1} > \tau_{\text{growth}}^{-1}$ with removal by either wind transport or sedimentation. When $\tau_{\text{remove}}^{-1}$ by wind transport is $> \tau_{\text{fall}}^{-1}$ and the cooling rate is dynamically controlled, i.e., $\tau_*^{-1} \sim \tau_{\text{remove}}^{-1}$, the cloud lifetime can exceed the lifetime of individual particles in the cloud because the condensing substance can be recycled from the cloud to the source/sink region and back to the cloud. A precipitating cloud forms when $\tau_{\text{remove}}^{-1} < \tau_{\text{growth}}^{-1}$. The size attained by these large particles is then either limited by $\tau_{\text{fall}}^{-1} = \tau_{\text{growth}}^{-1}$, or by disruptive collisions. The importance of evaporating precipitation depends on the conditions below the cloud. In some cases, the precipitation evaporates before reaching the surface, while in some

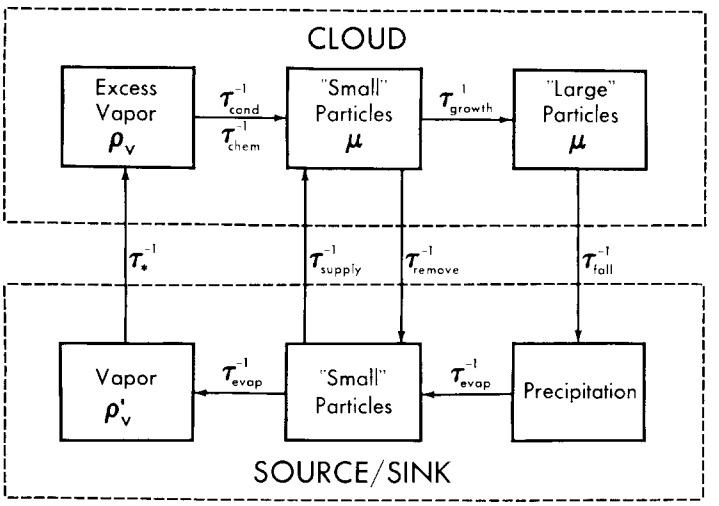

FIG. 1. Block diagram of a simple conceptual model of an aerosol or cloud. Symbols are defined in the text.

very violent storms, the precipitation can encounter strong winds that return it to the cloud. In other words, the growth history of particles in precipitating clouds can be very complicated.

(*iii*) *Chemical clouds.* This term refers to clouds which form when in situ chemical processes produce either a vapor density $\rho'_v > \rho_s$ at a rate, τ_*^{-1}, or very small particles at a rate, τ_{chem}^{-1}. In the former case, condensation follows and the cloud behaves like an ordinary cooling cloud, except that the time required to attain a balance between vapor supply and consumption is not necessarily short. In the latter case, rapid coagulation occurs and the cloud behaves like a dust cloud. I have separated this type of cloud from the others primarily because its properties are so poorly known. For instance, a choice between formation processes is not yet possible even for representatives of this cloud type in Earth's atmosphere.

The simple model of an aerosol or cloud, illustrated in Fig. 1, cannot completely represent the properties of any real cloud which is both spatially and temporally inhomogeneous. Further, this approach does not take account of feedback between the cloud microphysics and atmospheric dynamics. Instead, I intend to estimate the order of magnitude of the cloud and atmosphere properties in order to describe a "typical" cloud under "typical" atmospheric conditions. This approach is required by a shortage of information about aerosols in other planetary atmospheres.

III. NUCLEATION AND CONDENSATION

The discussion in this section is based on that of Frenkel (1946), Fuchs (1959), and Nielsen (1964), on reviews of Earth water clouds by Fletcher (1962), Mason (1971), Sedunov (1974), and Hobbs (1974), and on a review of the stratospheric sulfate layer by Castleman (1974). Dufour and Defay (1963) give a detailed treatment of cloud thermodynamics.

The characteristic time constant of the condensation growth of a population of particles is the time required for the population to e-fold its mass,

$$\tau_{cond}^{-1} \equiv \frac{1}{\mu}\frac{d\mu}{dt} = \left[\frac{d}{dt}\int Mn(M)dM\right] \times \left[\int Mn(M)dM\right]^{-1}. \quad (6)$$

With the mean mass defined as $\bar{M} = \mu/N$, (6) becomes

$$\tau_{cond}^{-1} = (\bar{M}N)^{-1}\int (dM/dt)n(M)dM + (\bar{M}N)^{-1}\int M[dn(M)/dt]dM. \quad (7)$$

The growth rate, τ_{cond}^{-1}, is equal to the growth rate of the particle masses plus the growth rate of the total number of particles. The latter quantity is just the nucleation rate.

A. *Nucleation Rate*

All nucleation theories assume the existence of an initial distribution of molecular embryos and express their properties as a function of size and ambient conditions. The usual property specified, following the classical homogeneous nucleation theory, is the free energy difference between molecules in an embryo and in the vapor. The most convenient description is a critical vapor density for each embryo size. Then, for a given vapor density, there is an embryo size for which $S = 0$ corresponding to the maximum in the free energy as a function of embryo size. The embryos larger than the critical size grow with $S > 0$ and the smaller embryos evaporate with $S < 0$, where S is given by

$$S = S_\infty - S_{curv} + S_{gas} + S_{ion} + S_{chem} + S_{CCN}. \quad (8)$$

The four theories of nucleation, each described by terms on the right side of (8), differ only in their embryo properties.

1. Homogeneous homomolecular nucleation. The embryos in the classical theory, based on the kinetic theory of phase changes, are a Boltzmann distribution of molecular aggregates formed by the statistical density fluctuations in an isothermal gas (Frenkel, 1946; Abraham, 1968). The nucleation rate is equal to the collision rate of the molecules in a perfect gas with the embryos times the number of embryos of critical size. There is also a correction factor to account for the evaporation of some molecules from the embryos. The number of critical embryos depends on the free energy of the molecules in the embryo which is modeled as a small liquid droplet. Since these small droplets have a finite surface area, the equilibrium vapor density is larger over these droplets than over a flat surface of condensate so that the effective supersaturation is smaller (Mason, 1971) by an amount, s_{curv}, in (8). The liquid droplet model does not adequately describe the embryo properties (Daee *et al.*, 1972), however, and further work is required. Experimental data show that homogeneous nucleation occurs only at very high supersaturations [e.g., $s_\infty \sim 5$ to 8 for water (Mason, 1971)], in qualitative agreement with the theory. Since nucleation by other processes occurs at much lower supersaturations, homogeneous nucleation is not expected in planetary atmospheres.

2. Heterogeneous nucleation on "small particles." Since the interaction of vapor molecules with other molecules can significantly reduce their free energy relative to interactions with each other, heterogeneous embryos, containing a chemically inert gas molecule or ion, nucleate at a higher effective supersaturation than homogeneous embryos. This is represented in (8) by the terms s_{gas} and s_{ion}. For example, nucleation on noble gas molecules (Allen and Kassner, 1969) or ions (Castleman, 1974) occurs at $s_\infty \sim 3$ to 5 for water. This process is also unlikely in planetary atmospheres except at extreme altitudes.

3. Chemical nucleation. Chemical nucleation refers to any gas phase chemical reaction which produces embryos from the vapor. One such process is heteromolecular nucleation, the nucleation of embryos from two or more gases which have solution-forming condensed phases. The nucleation rates of some water solutions have been calculated by extending homogeneous nucleation theory with composition dependent embryo properties (Stauffer and Kiang, 1974); however, the uncertainties involved are even larger than for homogeneous nucleation. The theory and experimental data, in qualitative agreement, show that the effective supersaturation for this type of nucleation is much larger by an amount $s_{chem} \gtrsim |s_\infty|$ in (8). In fact, nucleation can occur with s_∞ for each pure substance <0. There are also stronger chemical reactions, besides solution formation (e.g., hydration, oxidation, acid–base reactions), which produce large stable embryos even when $s_\infty \ll 0$ (Vohra and Nair, 1970) so that there is no subsequent condensation growth phase. These particles can only grow in response to an increase of the condensing vapor density. There is currently no theory describing this type of nucleation. Chemical nucleation seems to produce most of the submicron aerosols in Earth's atmosphere (Junge, 1963; Cadle and Grams, 1975) and is likely to occur in other planetary atmospheres as well.

4. Heterogeneous nucleation. The embryos in this theory contain or form on the surface of other small aerosols of varying composition and solubility in the condensate. These particles are called cloud condensation nuclei (CCN). The Volmer–Fletcher theory for embryos on the surface of insoluble particles (Fletcher, 1962) ex-

presses the change in the molecule free energy by interaction with the nucleus surface in terms of a contact angle between the vapor–liquid and liquid–surface interfaces. This geometric factor is a function of the surface energies (vapor–liquid, vapor–surface, liquid–surface) and makes the effective supersaturation for nucleation larger by an amount s_{CCN} in (8). If the CCN are soluble in the condensate, then the properties of the embryo are dependent on the solution strength, a function of the embryo size for a fixed CCN mass. Theoretical values of the critical supersaturation as a function of embryo size exist for dilute solutions (Mason, 1971), for some strong acid–water solutions (Vohra and Nair, 1971), and for embryos containing partially soluble CCN (Junge and McLaren, 1971). Experimental results for artifical and natural CCN (Twomey, 1959a,b; Junge and McLaren, 1971; Fitzgerald, 1973) show good qualitative agreement with these theoretical results, but closer agreement is not easily obtained because of the presence of adsorbed surface layers of gases and particulates (including organic compounds on Earth) which can drastically alter the nucleating efficiency of these particles (Podzimek and Saad, 1975). The primary conclusion from these studies is that this type of nucleation is very efficient, occurring at $s_\infty \sim 0$. Heterogeneous nucleation is thus a primary nucleation process in all planetary atmospheres.

5. Nucleation of ice. The general features of the nucleation theories discussed above apply to the nucleation of the solid phase from either the vapor or liquid phase, (Hobbs, 1974). In general, the crystalline structure of a growing ice embryo is much more sensitive to the presence of impurities than is a liquid embryo with its greater molecular mobility. The thermodynamic properties of these embryos are also much more difficult to calculate theoretically or to measure reliably, making comparisons between theory and experiment hard to evaluate. Although the agreement between theory and observations of water ice remains poor (Hobbs, 1974; Gerber, 1976), the observations do confirm the general theoretical results that heterogeneous nucleation is the most efficient process and that the CCN are less effective for nucleating the solid phase than the liquid phase; i.e., impurities stabilize the liquid phase relative to the gas and solid phases. As a result, ice nucleation at temperatures near the freezing temperature occurs by the nucleation of supercooled liquid droplets, at s_∞(liquid) $> s_\infty$(ice), followed by their rapid freezing (Hobbs, 1974). At much lower temperatures, ice nucleation is direct.

6. Nucleation rate. The two most effective nucleation processes, from the foregoing discussion, are chemical nucleation and heterogeneous nucleation, i.e., s_{chem} and s_{CCN} are $\gg s_{curv}$, s_{gas}, s_{ion} in (8). The production of *new* particles composed of relatively involatile substances in Earth's atmosphere, even though their total mass density is extremely low, argues in favor of some nucleation process other than heterogeneous nucleation which does not produce *new* particles (Twomey, 1977). However, so little is known about the chemical nucleation process that I can do no more than to suggest that it can be an important source of aerosols in all planetary atmospheres.

With a chemically produced or surface-derived population of submicron to micron size particles present in an atmosphere, the more abundant volatiles, such as water, can nucleate most effectively by the heterogeneous process. Since the growth of the embryos dilutes the effect of the CCN, s_{CCN} in (8) must decrease as embryo size increases. Stable embryos are then possible when $s_\infty < 0$ and $s = s_\infty + s_{CCN} = 0$. For example, most aerosols in Earth's lower atmosphere are $>10\%$ water by

mass even at low humidities (Ho *et al.*, 1974). Thus, heterogeneous nucleation in a "dirty" atmosphere is actually an "activation" of a preexisting population of condensate embryos when S increases above zero. In order to estimate the nucleation rate by this process, I assume that all other planetary atmospheres are as "dirty" as Earth's.

The nucleation rate is equal to $N^{-1}dN/dt$, the rate at which the number of activated particles increases. If the embryo size distribution is described by the supersaturation required to activate each size, i.e., $N = N(S_\infty)$, then $N^{-1}dN/dt \propto S_\infty^{-1}dS_\infty/dt$ and

$$dS_\infty/dt = (S_\infty + 1)\tau_{\text{cool}}^{-1} - \epsilon(S_\infty + 1)\tau_{\text{cond}}^{-1}, \quad (9)$$

where $\tau_{\text{cool}}^{-1} = -\rho_s^{-1}d\rho_s/dt$ and $\tau_{\text{cond}}^{-1} = \mu^{-1}d\mu/dt = -\mu^{-1}d\rho_v/dt$. The cloud mass density is $\mu = \epsilon\rho_v$, where $\epsilon < 1$. As S_∞ increases, the number of actively growing particles increases until their vapor consumption rate balances the rate at which excess vapor is produced by cooling; then, $dS_\infty/dt = 0$, S_∞ is a maximum, and nucleation ceases. Since heterogeneous nucleation is so efficient that $S_\infty \ll 1$, the order of magnitude of the nucleation time, the time required to reach maximum supersaturation, is $\tau_{\text{nuc}} \sim S_{\max}\tau_{\text{cool}}$, for a constant τ_{cool}. This estimate is correct since the second term in (9) increases monotonically during nucleation so that its average value must be less than its maximum value, τ_{cool}^{-1}.

Assuming $N(S) = \xi S^k$, Twomey (1959b) derives estimates for the maximum supersaturation, $S_{\max}$, and the particle number density, N_0, when $dS_\infty/dt = 0$:

$$S_{\max} \approx [(1/2\pi\xi)(\rho_p/\rho_s D^3)^{1/2}\tau_{\text{cool}}^{-3/2}]^{1/k+2} \quad (10)$$

and

$$N_0 = \xi S_{\max}^k \simeq \xi^{2/k+2} \times [(1/2\pi)(\rho_p/\rho_s D^3)^{1/2}\tau_{\text{cool}}^{-3/2}]^{k/k+2}, \quad (11)$$

where D is the vapor diffusion coefficient. For a very narrow CCN size distribution, $k \gg 1$, the number density of activated particles is determined almost entirely by the dynamics represented by τ_{cool}. In a constant mass cloud, a small updraft velocity (large τ_{cool}) produces a small value of $S_{\max}$ and N_0 resulting in a few large particles, while a large updraft velocity (small τ_{cool}) produces a large value of $S_{\max}$ and N_0 resulting in many small particles. In contrast, for a broad CCN size distribution, $k \lesssim 1$, the number density of cloud particles is almost proportional to the number density of CCN, represented by ξ, with little dynamic control (Twomey, 1977). These results are corroborated by more detailed numerical calculations [see Mason (1971) and Saad *et al.* (1976) for references].

Since there is little information about the number density and composition of CCN in other planetary atmospheres, i.e., about ξ and k, and only theoretical estimates exist for τ_{cool}, no reliable estimates of $S_{\max}$ and N_0 can be made. However, $S_{\max}$ is such a weak function of these parameters that it remains nearly constant over a wide range of conditions (Braham, 1976). Therefore, since most of the cooling clouds that I consider here are water clouds, I assume that water clouds in Earth's atmosphere are typical of the other cooling clouds in similarly "dirty" atmospheres. Consequently, I adopt the value $S_{\max} = 10^{-3\pm1}$ and leave N_0 undetermined for all the calculations. The efficiency of heterogeneous nucleation which keeps $S_{\max} \ll 1$ is also expressed in the result that $\tau_{\text{cool}} \sim \tau_{\text{cond}} \gg \tau_{\text{nuc}}$, where the condition $\tau_{\text{cool}} \sim \tau_{\text{cond}}$ obtains because most of the vapor is converted to cloud particles, i.e., $\epsilon > 0.1$.

7. Nucleation of involatile substances. The discussion above is based primarily on the study of condensing volatiles, substances such as water with equilibrium vapor densities at atmospheric tempera-

tures that are only a few orders of magnitude smaller than the atmospheric density. For these substances the nucleation rate is dominated by an exponential dependence on the supersaturation; hence the effective value of S for rapid nucleation remains small and there is no explicit dependence on the absolute vapor density. This is not true for the condensation of involatile substances which have equilibrium vapor densities at atmospheric temperatures that are many orders of magnitude smaller than the atmospheric density. For example, sulfuric acid has $\rho_s \ll 10^{-10}\,\rho$, typically. In this case, the nucleation rate depends on the collision rate between vapor molecules controlled by the vapor density. Even a moderate nucleation rate then, requires extremely high supersaturations (Twomey, 1977). The condensation of such substances requires much more study.

B. Growth Rate of a Single Liquid Droplet

The mass increase of a single liquid droplet, dM/dt in (7), depends on the net flux of vapor molecules to the droplet surface. Since the latent heat of the phase change raises the droplet temperature and the equilibrium vapor density near the droplet, the net flux of vapor molecules is influenced by the net flux of this excess heat away from the droplet. The classical diffusion theory for these fluxes models the molecular motions as a random walk all the way down to the droplet surface. Chandrasekhar (1943) shows that the characteristic time and length scales of the fluxes must be much larger than the time and length scales associated with the molecular motions to insure the validity of this diffusive description. These conditions are equivalent to the condition that $\mathrm{Kn} \ll 1$. This guarantees that a vapor molecule spends many collision times within one droplet radius of the droplet surface, making the droplet growth insensitive to the sticking efficiency of the vapor molecules. Mason (1971) derives the classical Maxwell growth rate by assuming a diffusive mass and heat flux, and a small droplet–atmosphere temperature difference:

$$G(M) \equiv (1/M)dM/dt = [4(3)^{1/2}\pi\rho_p]^{2/3} \times (\rho_s/\rho_p)S\mathfrak{D}M^{-2/3}. \quad (12)$$

The effective mass diffusion coefficient is

$$\mathfrak{D} = D[1 + \rho_s DL(Lm_v/kT - 1)/\kappa T]^{-1}, \quad (13)$$

where κ is the thermal diffusion coefficient and the factor in brackets corrects the classical mass diffusion coefficient, D, for the latent heat effect. This factor is ~ 1 for all the situations considered in this paper, i.e., the droplet temperature never differs significantly from that of the atmosphere. Meyer's formula for D is (Fuchs and Sutugin, 1970)

$$D = \tfrac{1}{3}\bar{v}\lambda = \tfrac{2}{3}f\eta/\rho, \quad (14)$$

where $\bar{v}$ is the mean thermal velocity of the molecules and f corrects for the finite mass of the vapor molecules. The value of f is ≈ 2 for water vapor on Earth, Venus, and Mars, ≈ 3 for sulfuric acid vapor on Earth and Venus, and ≈ 5 for water and ammonia vapor on Jupiter. The value of D in (14) is the steady-state value which neglects the counter-flow of the background gas away from the droplet to maintain constant total pressure. Fuchs (1959) shows that this value is appropriate when $\rho_v \ll \rho$ and $\mathrm{Re} \ll 1$ for the droplet's motion. The former condition is met in all cases studied here. When $\mathrm{Re} > 1$, the diffusion coefficient is corrected by a ventilation factor, F. Several values of F have been suggested (cf. Fuchs, 1959; Watts, 1971; Mason, 1971) but the available experimental data are consistent with the simpler empirical expression $F = 1 + 0.2\,\mathrm{Re}^{1/2}$ (Mason, 1971).

In the gas kinetic regime, $\mathrm{Kn} \gg 1$, the mass flux to the droplet and the heat flux

away from the droplet are modeled by collisions between a Maxwell–Boltzmann gas and a stationary droplet (Fuchs, 1959; Brock, 1966; Fukuta and Walter, 1970). The resulting expression for the droplet growth rate is the same as (12) with D replaced by $\alpha a(8kT/\pi m)^{1/2}/4$ and the second term in brackets in (13) multiplied by $(\alpha/\alpha')(\kappa/\rho D)(C_v + R/2)^{-1}$. The molecular sticking efficiency, α, is also called the condensation coefficient (Fukuta and Walter, 1970). In contrast to the classical regime, the time a molecule spends near the droplet surface in this regime is very short with the consequence that the growth rate is linear in α. The heat flux efficiency factor, α', also called the accommodation coefficient, accounts for the efficiency with which rebounding gas molecules are thermalized. (In very tenuous atmospheres, the radiative heat flux can become significant, but this effect is small for the clouds considered here.) While the experimental values of α and α' are not in good agreement (cf. Fuchs, 1959; Warner, 1969; Fuchs and Sutugin, 1970; Fukuta and Walter, 1970; Carstens *et al.*, 1974), the data suggest that $\alpha < \alpha'$, i.e., the condensation coefficient is the most important factor determining the growth rate.

Since the motions of the vapor molecules near the droplet surface in the intermediate regime, Kn $\sim$ 1, are neither strictly diffusive or kinetic in character, a general theory of the growth rate in this regime does not exist. Several approximate expressions with limited validity and success have been proposed (Fuchs, 1959; Brock, 1966; Fuchs and Sutugin, 1970; Fukuta and Walter, 1970; Carstens *et al.*, 1974) which are all consistent with a formal joining of the classical and gas kinetic expressions. This formal expression for the growth rate is

$$G(M) \approx [4(3)^{1/2}\pi\rho_p]^{2/3}(\rho_s/\rho_p)\mathcal{S}M^{-2/3} \times D(1 + 4\mathrm{Kn}/3\alpha)^{-1}, \quad (15)$$

where α can be modified to account for small values of α' (Carstens *et al.*, 1974). A small value of α can significantly decrease the droplet growth rate even if Kn is small. For convenience, I assume $\alpha = 1$, but consider the consequences of $\alpha \ll 1$ in each case.

C. Growth Rate of a Single Solid Particle

The growth of the solid phase produces highly elongated shapes because the growth rate is extremely sensitive to conditions on the surface of the growing particle. On a growing water ice crystal, e.g., the vapor molecule sticking efficiency is a function of the position in the crystal structure with the consequence that some crystal facets grow more rapidly than others. Just which facets grow most rapidly is not only a sensitive function of temperature, but also easily altered by impurities (Hobbs, 1974). In spite of this complexity, (15) is a good estimate of the mass growth rate of the ice crystal if the particle radius represents the radius of the equivalent mass sphere and the correct value of α is used. Experimental values of α do not yet agree (Hobbs, 1974), but recent results for water ice give $\alpha \sim 10^{-3}$ for temperatures well below freezing (Choularton and Latham, 1977).

At temperatures below but near the freezing temperature, ice nucleates as supercooled liquid droplets that rapidly freeze. The effective supersaturation during the subsequent condensation growth is much greater then, because $\mathcal{S}_\infty$(liquid) $> \mathcal{S}_\infty$(solid) below the freezing temperature. In this situation, the growth rate of ice is much higher than typical for growth of the liquid phase above the freezing temperature or the solid phase far below it. I approximate this effect by assuming $\mathcal{S}_{max} = 10^{-2\pm1}$ under these circumstances.

D. Growth Rate of a Population of Particles

For cooling clouds, heterogeneous nucleation is so efficient that the time re-

quired to complete the nucleation is much shorter than the subsequent growth phase, especially if the initial embryo mass is much smaller than the final cloud particle mass. For chemical clouds, there is no way to estimate the nucleation rate except to argue that either the rate is so rapid that all the vapor is converted to particles without a subsequent growth phase or the rate is so slow that the first few embryos consume all of the vapor. Since the growth rate of very small particles is much more rapid than that of larger particles, the nucleation phase still cannot contribute substantially to the total growth time. Therefore, the growth rate of particles much larger than the initial embryos is approximately equal to the growth rate evaluated after the nucleation phase.

When nucleation ceases, the particle number density is constant. τ_{cond}^{-1} in (7) then reduces to $\bar{M}^{-1}d\bar{M}/dt = G(\bar{M})$, the growth rate of a single particle with the mean mass. Substitution of $G(\bar{M})$ for τ_{cond}^{-1} in (9) shows that the second term is proportional to $\mathcal{S}\bar{M}^{-1/3}$. Thus, although a precise balance between the two terms is not possible because an increasing mean mass requires a decreasing supersaturation, the variation of $\mathcal{S}$ is very slow. I assume, consistent with the approximate value of $\mathcal{S}_{\max}$, that $\mathcal{S} \sim \mathcal{S}_{\max}$ is constant during the growth phase of the cloud.

The expressions for τ_{cond} in the remainder of this paper are

$$\tau_{\text{cond}}^{-1} = \rho^{-1}a^{-2}(2f\eta\rho_s\mathcal{S}_{\max}/\rho_p)$$

for $\text{Kn} \ll \alpha$ (16)

and

$$\tau_{\text{cond}}^{-1} = a^{-1}(3\alpha f\rho_s\mathcal{S}_{\max}/2\rho_p)(2kT/\pi m)^{1/2}$$

for $\text{Kn} \gg \alpha$, (17)

where a is the particle radius corresponding to the mean particle mass. Equation (16) is modified by the ventilation factor when Re for the particle terminal velocity exceeds $\sim 10^2$.

If condensation with constant $\mathcal{S}_\infty$ is the only process acting on the cloud particles, then the particle size distribution that results is very narrow for two reasons. The first is that the size dependence of the other terms in (8) causes different size particles to grow at different rates. Although the particle surface effects, represented by $\mathcal{S}_{\text{curv}}$ as well as α and Kn, all retard the growth of small particles (<10 μm), the impurity effects, represented by the rest of the terms in (8), enhance the growth of these small particles (Rooth, 1960). In general, the latter effect is stronger in a "dirty" atmosphere. The second reason is that, for large particles for which the impurity effects are negligible, τ_{cond} in (16) increases as the radius squared so that the smaller particles soon catch up to the larger particles. This produces a very narrow size distribution and uniform growth rate (Fitzgerald, 1972; Saad *et al.*, 1976).

E. Summary and Comments

The estimates for the condensation growth time of a population of particles in (16) and (17) are good if all the properties of heterogeneous nucleation in "dirty" atmospheres apply to other planetary atmospheres. These properties are that heterogeneous nucleation is (a) so efficient that $\tau_{\text{nuc}} \ll \tau_{\text{cond}}$ and $\mathcal{S}_{\max} \ll 1$, (b) so insensitive to the properties of the CCN and the dynamics that $\mathcal{S}_{\max} = 10^{-3\pm1}$, and (c) sufficiently inefficient for ice nucleation that $\mathcal{S}_{\max} = 10^{-2\pm1}$ for growth near the freezing temperature.

There is one situation for which the small values of $\mathcal{S}_{\max}$ are incorrect. Since $\mathcal{S}_\infty(\text{ice}) < \mathcal{S}_\infty(\text{liquid})$ at the same temperature below freezing, the presence of both phases in a cloud results in the rapid evaporation of the liquid droplets and growth of the ice particles. This process,

called the Bergeron process, occurs when the droplets in a growing cloud are carried above their freezing level by strong vertical motions, and rapidly produces very large particles. The Bergeron process is an important step in producing rain in mid-latitude thunderstorms on Earth (Mason, 1971; Twomey, 1977); e.g., for water droplets and water ice at 263°K, $s \sim 10^{-1}$.

An important difference between the simple cloud particle population, discussed thus far, and a more realistic population is that the latter is a function, not only of time, but also of location within the cloud. Although careful observations of water clouds on Earth confirm the existence of the narrow condensation-produced droplet size distribution near the cloud bottom (Fitzgerald, 1972), the typical size distribution in the main part of the cloud is broad, even bimodal (Warner, 1969; Mason, 1971). The most likely explanation for these distributions is turbulent effects (Latham and Reed, 1977). Turbulence causes varying cooling rates and vapor densities (mixing with drier air), cycles a volume of the cloud through repeated heating and cooling episodes, and mixes volumes of the cloud with different size distributions. The resulting complex size distribution is certainly very different from that produced by condensation alone. However, since the only available observations of other clouds are estimates of the particle mean size, the simple order of magnitude estimates made here are sufficient.

IV. PARTICLE MOTION

This section is a discussion of the important particle motions caused by gravity and atmospheric motions, called sedimentation and wind transport–surface interactions. The other important particle motion, the Brownian motion of the smaller particles caused by molecular forces, is discussed in Section V. The particle motions caused by other forces, e.g., electrical forces, are generally comparatively weak, although they can introduce some important modifications of the efficiency of the processes considered in this paper. These effects are discussed qualitatively.

A. *Sedimentation*

The sedimentation time constant, τ_{fall}, is here defined as the time for a particle to fall one atmospheric scale height at its terminal velocity, V. Since the theory of the terminal velocity of a rigid sphere in a gas is more familiar than others discussed in this paper, I only briefly summarize the important facts and discuss the differences between the behavior of rigid spheres and actual aerosol particles. [For more complete reviews, see Fuchs (1964), Fuchs and Satugin (1970), Berry and Pranger (1974), Chamberlain (1975), and Beard (1976).]

1. The well-known Stokes expression for the terminal velocity of a rigid sphere is

$$V = 2\rho_p g a^2/9\eta. \tag{18}$$

This expression is valid when $\text{Kn} \ll 1$ and $\text{Re} \ll 1$.

2. The variation of the terminal velocity with Kn is accurately described by the Cunningham factor, $1 + \beta\text{Kn}$, with $\beta \approx \frac{4}{3}$ over all Kn (Berry and Pranger, 1974).

3. The variation of the terminal velocity with low and intermediate values of Re ($\text{Re} \lesssim 70$) is described by the factor, $1 + (C_D\text{Re}/24)^{-1/2}$, where the drag coefficient is $C_D = C_0(1 + 9.06\ \text{Re}^{-1/2})^2$ (Abraham, 1970). This is valid when $\text{Kn} \ll 1$.

4. For $\text{Re} \gg 70$, the drag coefficient is roughly constant, $C_D \approx 0.2$ (Prandtl, 1953).

The sedimentation time constant in

three regimes is

$$\tau_{\text{fall}} = 9\eta kT/2\rho_p mg^2a^2$$

(Re $\ll$ 70, Kn $\ll$ 1),

$$\tau_{\text{fall}} = [3\rho(kT)^2/40\rho_p m^2g^3a]^{1/2}$$

(Re $\gg$ 70, Kn $\ll$ 1),

$$\tau_{\text{fall}} = 27\pi\rho(2kT/\pi m)^{3/2}/16\rho_p g^2 a$$

(Kn $\gg$ 1). (19)

The atmospheric scale height is $H = kT/mg$. The particle size for which Re = 70 is

$$a^2 = 9C^*\eta^2/4\rho_p\rho g, \quad (20)$$

where the dimensionless drag coefficient which corresponds to Re = 70 is $C^* \equiv C_D\text{Re}^2/24 = 270$ (Berry and Pranger, 1974).

Since liquid droplets are not rigid, their terminal velocities differ from that of rigid spheres because they can support internal circulations and large distortions of shape without disruption. The first effect, measured by the ratio of the gas to liquid viscosity, can be neglected since the viscosity of liquids is generally much larger than that of gases. The second effect is measured by the value of the Weber number. When We $\ll$ 1, the terminal velocities of liquid droplets are identical to that of rigid spheres. When We $\gg$ 1, the droplets fall more slowly than spheres. For example, 4-mm raindrops fall at half the terminal velocity of 4-mm spheres with the same density. Equation (19) is a lower limit to τ_{fall} for the very largest droplets.

The droplet size for which We $>$ 1 is

$$a^5 > 81\sigma\eta^2/2\rho_p^2g^2\rho$$

(Re $\ll$ 70, Kn $\ll$ 1),

$$a^2 > 3\sigma/20\rho_p g$$

(Re $\gg$ 70, Kn $\ll$ 1),

$$a^3 > 729\sigma kT\rho/16\pi\rho_p^2g^2m$$

(Kn $\gg$ 1). (21)

The largest droplets are so distorted when falling that they are disrupted by the growing Taylor instability of their lower surfaces. This occurs when the lower surface radius is larger than one-quarter of the wavelength of the lowest order oscillation of the droplet (Pruppacher and Pitter, 1971); hence, a is less than

$$a_{\max}(\text{hydro}) \approx (\pi/2)[\sigma/g(\rho_p - \rho)]^{1/2}. \quad (22)$$

This has been confirmed experimentally.

The terminal velocities of solid aerosol particles differ from that of spheres for two reasons. First, the structure of a solid particle can be quite porous so that the particle's mean density is much smaller than the bulk density of the material it is made of. Consequently, such a "snow" particle has a much smaller terminal velocity than that of a low porosity particle (a grain) of the same size. Second, hydrodynamic forces on the irregular shapes of solid particles tend to orient them in the maximum drag position, decreasing their terminal velocity below that of an equivalent volume sphere. In the Stokes flow regime, the drag is not a sensitive function of the particle shape. Moreover, the Brownian rotation of very small particles ($a < 10$ μm) overcomes the hydrodynamic orientation causing the particle to present an "average," more nearly spherical, cross section to the flow (Fuchs, 1964). In the high Re flow regime, the drag is more sensitive to particle shape; but for particles with aspect ratios <5, the terminal velocity is within an order of magnitude of that of a sphere (Prandtl, 1953; Hobbs, 1974). For particles with larger aspect ratios, the direction of maximum drag differs from the direction of motion causing the particles to side-slip or glide (Fuchs, 1964). This effect reduces the vertical component of the particle's velocity well below its terminal velocity. Thus (19) is a good estimate of τ_{fall} for

small grains and snow particles, if the porosity is known, and only a lower limit on τ_{fall} for large, highly elongated particles.

B. Wind Transport—Surface Interaction

Since atmospheric motions are fully turbulent, i.e., motions exist on all length scales from the planetary down to the viscous dissipation scale $\sim$1 cm, a cloud of intermediate size experiences both a steady wind (the larger scales of motion) and a variable wind (the smaller scales of motion). The motion of the cloud particles in a steady wind cannot be treated by the simple addition of velocities because the drag on the gas flowing through a cloud of even modest density greatly exceeds the drag on the gas flowing around the whole cloud (Fuchs, 1964). This means that the flow velocity through the cloud which determines the particle velocities can be slower than the wind velocity, the difference depending on the cloud size and density. Consequently, the cloud does not necessarily move with the wind velocity. Examples of the complications that this effect can introduce are observed in dense precipitating clouds on Earth where the updraft velocity driven by buoyancy forces is decreased by an increasing particle load and can be changed to a downdraft by heavy precipitation. Since even the large scale motions in other planetary atmospheres are poorly known, I consider only the qualitative effects of steady winds. The most important of these is that a steady updraft, associated with a cooling cloud, increases the lifetime of the cloud particles against sedimentation.

The effects of the smaller scale atmospheric motions on cloud particles are also difficult to predict in the absence of any knowledge of these motions in other planetary atmospheres. Furthermore, despite many theoretical and experimental studies of atmospheric turbulence (e.g., Sutton, 1953; Pasquill, 1974) and its effectiveness for particle transport (e.g., Meek and Jones, 1973; Pasquill, 1974; Caporaloni *et al.*, 1975), the general validity of these theories in other atmospheres is not yet established. Therefore, only an order of magnitude estimate of the lifetime of particles against turbulent transport is possible. The usual diffusive analogy suggests that the turbulent transport rate over a distance, L, is $\tau_{eddy}^{-1} \sim E/L^2$, where E is the eddy diffusivity; however, this estimate can be easily an order of magnitude in error, especially since it neglects the changing effectiveness of turbulent transport with particle size.

A measure of this effectiveness is the Stokes number which represents how readily a particle responds to accelerations in the gas flow past it. The gas drag for accelerated motion differs from that of steady motion because of the acceleration of the gas near the particle, but Fuchs (1964) shows that the difference is negligible when $\rho_p \gg \rho$ at low Re. This has been verified experimentally for water droplets up to Re $\sim$ 5 (Sartor and Abbott, 1975). For higher Re up to $\sim 10^3$, experimental results suggest that the Stokes (Re $<$ 1) drag coefficient is a better approximation than the nearly constant steady flow drag coefficient for high Re, which fails to predict decreasing drag with increasing Re (Fuchs, 1964). Using the Stokes drag coefficient to determine the stopping distance, d, in (4), Fuchs (1964) finds

$$\boxed{\text{Stk} = 2\rho_p a v/9\eta = \rho_p \text{Re}/9\rho,} \quad (23)$$

where $v = u$; the rms magnitude of the velocity variations in the turbulence. Since $\rho_p \gg 9\rho$ generally, Stk $\gg$ 1 for particles with Re $>$ 1. These larger particles are not as effectively transported by turbulent motions as are smaller particles. (On Earth, e.g., the cutoff size is approximately 10 μm.)

The interaction of turbulent atmospheric

motions with planetary surfaces is both an important source and sink of aerosols. [See reviews in Bagnold (1941), Fuchs (1964), and Iversen *et al.* (1976).] If the typical surface winds in an atmosphere were extremely weak or the surface extremely smooth, then a very thick laminar boundary layer would exist near the surface (Prandtl, 1953) and particle deposition would occur by Brownian diffusion, inertial deposition, or sedimentation (Fuchs, 1964; Davies, 1966). However, the typical surface winds are strong enough and the surfaces (even deserts and oceans) are rough enough over a wide range of length scales that the winds are fully turbulent all the way down to the surface. Thus, the smaller aerosol particles are deposited by direct impact on surface obstacles at a rate that depends on the turbulent wind velocities (Fuchs, 1964; Davies, 1966; Chamberlain, 1975). Since the theories relating the mean atmospheric wind velocities to the surface wind velocities and turbulent velocities involve an empirical parameter, the friction velocity, u_*, their applicability to other atmospheres and surfaces is uncertain. As an order of magnitude estimate of the turbulent wind velocities, I use Sutton's (1953) rule that $u' \sim u_* \sim \bar{u}/10$, where $\bar{u}$ is the mean wind velocity well above the surface. The deposition flux for smaller particles (defined by $V < u'$) is, then, $\lesssim Nu'$. For very small particles ($<10^{-5}$ cm), for which $\mathrm{Stk} \ll 1$, even this deposition process is inefficient (Twomey, 1977). For larger particles ($V > u'$), the deposition flux is the sedimentation flux $\approx NV$ (Davies, 1966; Pasquill, 1974; Gillette *et al.*, 1974; Chamberlain, 1975).

Even though the motion and direct entrainment of the smaller particles in the soil on carefully prepared surfaces is initiated by smaller wind stresses than required for the larger particles (Sagan and Bagnold, 1975), direct entrainment of the smaller particles is strongly inhibited on natural surfaces by cohesive forces between particles and aerodynamic shielding of the smaller particles both by larger particles and by surface roughness features. Furthermore, the large scale roughness of a natural surface limits the wind stress to values, such that the first particles to move cannot be suspended by that wind (Bagnold, 1941; Chepil and Woodruff, 1963). During their ballistic flight, these first-moved particles attain the mean wind speed and give up this extra momentum in collision with particles on the surface. It is this transfer of wind momentum to the surface by these saltating particles that limits the wind momentum and also efficiently injects all soil particles into the atmosphere (Bagnold, 1941). The size distribution of the suspended particles with $V < u'$ is therefore the same as that of the parent soil without the larger particles (Bagnold, 1941; Chepil and Woodruff, 1963; Gillette *et al.*, 1974). With $u_* \sim u'$, Bagnold's (1941) estimate for the saltating mass flux is $\sim \rho u'$. The entrainment flux is then just the small to large particle mass ratio, ϵ, times the saltation mass flux. An upper limit to the mass density, $\bar{M}N$, attained in a dust storm is set by the equality of the entrainment and deposition fluxes: $\bar{M}N \sim \epsilon\rho$.

C. Summary

The importance of the sedimentation and wind transport processes is that they determine the lifetime of aerosol particles in an atmosphere and, therefore, they limit the action of all other particle processes. In general, turbulent wind transport decreases the lifetime of particles in a cloud from the value set by sedimentation. In a steady-state or decaying cloud, the net particle flux must be downwards and is determined by the operative process at the bottom of the cloud. Since the flux must be at least as large as the sedimentation flux, τ_{fall} at the bottom of the cloud

is an upper limit on the particle lifetime. Turbulence can only increase the downward flux out of the cloud thereby decreasing the particle lifetime. In a very deep cloud system with sedimentation at the bottom, τ_{fall} in the upper portion of the cloud is less than τ_{fall} at the bottom so that turbulence does increase the lifetime of the particles in the upper portions of the cloud but not in the cloud as a whole. Only in a growing cloud can the net particle flux be upwards. In this case, turbulent transport opposes sedimentation and temporarily increases the particle lifetime. Except for this special case, τ_{fall} is a strict upper limit on the typical lifetime of particles in a cloud.

V. PARTICLE COLLISIONS

Since it is difficult to specify the precise position and motion of every particle in an aerosol undergoing collisions, these collisions are usually described by a stochastic equation. This equation describes the time rate of change of a probability density function, $n(M, t)$, defined as the probability of finding a particle with mass between M and $M + dM$ in a unit volume at a time between t and $t + dt$ (Berry, 1967; Scott, 1967). The physical significance of this function and the validity of the stochastic collection equation are extensively debated in the literature (e.g., Bayewitz *et al.*, 1974; Gillespie, 1975). Scott (1967) shows that, to first order in the volume, $n(M, t)$ is identical to a physical number density distribution function, while Bayewitz *et al.* (1974) show that this same interpretation is proper for describing the mean behavior of the particle population.

In this paper, the collision time constant is defined as $N^{-1}dN/dt$. This is equivalent to a mass growth rate, since collisions conserve total mass. dN/dt is the integral of the usual stochastic collection equation, plus terms for particle disintegrations and other sources and sinks of particles, over the particle size distribution. Thus, the precise interpretation of $n(M, t)$ is not important here. The form of the collection equation used here is, after some simplification,

$$dN(t)/dt = \int_0^\infty dM n(M, t) \int_0^\infty dM' n(M', t) \times R(M, M') \{ -\tfrac{1}{2} P_1(M, M') + P_2(M, M')[J(M, M') - 1] \} + I_1(t) + I_2(t). \quad (24)$$

The first term represents the particle collisions, the second term represents particle disintegration, and the third term represents any other sources and sinks of particles. The processes that contribute to these last two terms have been discussed in earlier sections. $R(M, M')$ is the probability per unit time of a collision between particles with masses M and M', $P_1(M, M')$ is the probability that the collision results in the formation of a single particle of mass $M + M'$, $P_2(M, M')$ is the probability that the collision results in the disruption of one or both of the particles, and $[J(M, M') - 1]$ is the net total number of particles of mass M produced in a disruptive collision between particles with masses M and M'. A third possible outcome of a collision, with probability $P_3 = 1 - P_1 - P_2$, is that the two particles bounce apart after the collision with no change in $N(t)$. When $P_1 = 1$, (24) reduces to the usual integrated stochastic collection equation.

Many approximate treatments of the stochastic collection equation are discussed in the literature (e.g., Hidy, 1965; Friedlander and Wang, 1966; Berry, 1967; Liu and Whitby, 1968; Scott, 1968; Walter, 1973; Berry and Reinhardt, 1974; Gillespie, 1975; Scott and Levin, 1975). An important discovery by Friedlander and his colleagues is the existence of similarity solutions to the equation with $I_1 = I_2 = P_2 = P_3 = 0$. In particular, they find

that for Brownian coagulation, the normalized size distribution evolves towards the same invariant shape with constant variance regardless of the initial conditions, while the total number density and mean particle mass continue to change with time (Friedlander and Wang, 1966). Approximate similarity solutions also exist for more realistic forms of $R(M, M')$ as suggested by results obtained by Liu and Whitby (1968), by the numerical results of Hidy (1965) and Walter (1973) for coagulation, and by the numerical results of Berry and Reinhardt (1974) for coalescence. Thus collision controlled aerosols should exhibit a characteristic size distribution shape, somewhat broader than that of condensation dominated aerosols, but still quite narrow.

Numerical solutions of the stochastic collection equation with simple models of disruptive collision processes confirm the intuitive conclusion that a steady-state size distribution is attained when the growth of large particles from smaller particles is balanced by the collisional disruption of these larger particles back into smaller particles (Srivastava, 1971; K. C. Young, 1975). There are only a few observations of water droplet disruptions (e.g., McTaggart-Cowan and List, 1975) and no quantitative theories for this process. The influence of disruptive collisions is simply and adequately modeled here by stopping the collision growth of the mean particle size when it reaches the size at which collisions become disruptive. Therefore, I simplify (24) by replacing the factor in braces by a sticking efficiency, $s = 1$ when growth is occurring and $s = 0$ when either bouncing or disruption predominates.

A. *Sticking Efficiency*

1. Solid particles. Because of the short range of molecular forces, the binding energy of a single particle in which the molecules interact over distances of a few angstroms is much larger than the binding energy between two solid particles, for which the surface curvature and roughness greatly increase the interaction distance. Consequently, colliding solid particles only bounce apart and $s = 0$ over the large intermediate range of collision kinetic energy where it is too large for sticking to occur but too small for disruption to occur.

An estimate of the upper limit on the mean size of a colliding particle population is obtained by equating the collision kinetic energy to the energy required to split a particle in two. With a typical molecular bond length $\sim 10^{-8}$ cm and an energy per bond ~ 3 eV, the collision kinetic energy exceeds the splitting energy when

$$\boxed{a > (3 \times 10^4)\rho_p^{-1} v^{-2} \text{ cm.}} \qquad (25)$$

Although the energy required to break off smaller pieces of the particles is smaller than that used in (25), the collision kinetic energy is not converted to splitting energy with perfect efficiency. These offsetting effects make (25) a good order of magnitude estimate of the maximum size of colliding solid particles, especially since only fragments with masses of order the original particle masses can contribute to the size distribution.

The particle size at which sticking becomes efficient is estimated by equating the binding energy between two particles and their collision kinetic energy. If the two colliding particles are idealized as spheres which approach to within a distance, δ, then the binding energy of the Van der Waals force between surface molecules or with thin liquid films on their surfaces is $\sim \pi Q a/\delta$ (Fuchs, 1964). Q is a measure of the strength of the interaction potential while δ is determined by the scale of small, surface roughness elements or the liquid film thickness. In order for sticking to occur, then, this

binding energy must exceed the collision kinetic energy, i.e.,

$$a^2 < \tfrac{3}{2}\pi Q \rho_p^{-1} \delta^{-1} v^{-2} \text{ cm}^2. \quad (26)$$

Although the rebound kinetic energy is generally somewhat smaller than the initial kinetic energy, this estimate is still correct within an order of magnitude. The meager experimental evidence available from studies of solid aerosols sticking to the walls of air ducts and to filters suggests that $Q \sim 10^{-14}$ to 10^{-13} erg, with only a weak dependence on composition and particle size, and $\delta \sim 10^{-8} - 10^{-6}$ cm (Fuchs, 1964; Davies, 1966; Corn, 1966). With these values (26) is consistent with

$$\boxed{a^2 < 10^{-6} v^{-2} \text{ cm}^2.} \quad (27)$$

For coagulating aerosols, the kinetic energy of Brownian motion is approximately $3kT/2$. The corresponding value of the collision velocity in (25) and (27) gives $a < \sim 10^{-9}$ cm and $a > \sim 10^{-8}$ cm, respectively. Particles this size are individual molecules and atoms for which these estimates are probably not correct, but this result implies that the sticking efficiency for coagulation is unity with no disruptive collisions except for very small particles ($a \lesssim 10^{-7}$ cm) or very high temperatures ($T > 10^3$ °K) (Fuchs, 1964). Clearly, since there is an energy barrier to condensation, coagulation cannot be effective for molecules.

For coalescing aerosols, the collision velocity in (25) and (27) is approximately equal to the terminal velocity of the particles. Generally, the particle size given by (27) is so small for solid aerosols that hydrodynamic forces prevent collisions between those particles which can stick together (see Part C). The particle size given by (25) is so large (>100 μm) that few particles of this size are expected to occur in planetary atmospheres. Thus solid aerosols do not grow by coalescence.

The one important exception to this conclusion is the coalescence of solid condensates. Unlike dust grains, ice particles have highly elongated or intricate shapes with much lower terminal velocities than their masses suggest. Consequently, the cutoff radii in (25) and (27) are much larger for ice crystals. Further, once collisional growth begins, the composite snow particles that form are so porous that their terminal velocities deviate even further from those of equal mass spheres. On Earth, water ice crystals grow efficiently by coalescence into very large (~ 1 cm), porous (mean density $\sim 0.1\rho_p$) particles built from numerous whole and broken crystals (Jiusto and Weickmann, 1973; Hobbs, 1974). There are further complications, such as freezing liquid films and breaking in the porous structures, that cannot be accounted for even qualitatively, but the behavior of snow on Earth suggests that $s \approx 1$ for the coalescence of ice up to radii ~ 1 cm.

2. Liquid droplets. In contrast to solid particles, the high mobility of molecules in two colliding liquid droplets allows them to form a single droplet upon contact. The relevant binding energy is then just the surface energy of the single droplet. If the collision kinetic energy is much smaller than the surface energy, the sticking efficiency is unity, whereas if it is much larger than the surface energy, the droplet is disrupted and $s = 0$. This is expressed by the ratio of the collision kinetic energy to the droplet surface energy, called the collision number

$$\text{Cn} = \rho_p a v^2 / 6\sigma, \quad (28)$$

where $s = 1$ when $\text{Cn} \ll 1$ and $s = 0$ when $\text{Cn} \gg 1$.

The behavior of colliding droplets in the transition regime, $0.1 \lesssim \text{Cn} \lesssim 10$, is more complicated than the simple bouncing regime for solid particles. Two modes of droplet instability produce a dependence of the critical value of Cn for sticking on the collision impact parameter expressed

as a fraction of the geometric collision cross-sectional area. In collisions with impact parameters $\gtrsim 0.5$, most of the kinetic energy becomes rotational energy in the resultant droplet. Theory and experiment show that rotational disruption occurs for two equal colliding droplets when $\mathrm{Cn} \gtrsim 1$ at impact parameters near unity (Brazier-Smith *et al.*, 1972). For smaller impact parameters and droplet radius ratios, the critical value of Cn rapidly increases towards 10 because the angular momentum of the collision sharply decreases. In collisions with impact parameters $\lesssim 0.5$, or small droplet radius ratios, most of the kinetic energy goes into radial motions at the impact equator. When the energy of these motions exceeds the droplet surface energy, many small droplets form and move rapidly away from the impact equator (Gunn, 1965). Estimates of the critical surface energy calculated from the surface energies of distorted, but axisymmetric, droplet shapes (Brazier-Smith *et al.*, 1972) suggest a critical value of $\mathrm{Cn} \sim 10$ for this disruption mode.

A further complication in this regime is that the droplets can rebound from a collision without disruption as long as contact between the droplets is prevented. When the rebound time is smaller than the time required for the intervening gas layer to drain, the droplets never touch and bounce apart (Foote, 1975). Since the draining time monotonically increases with droplet radius (Fuchs, 1964) while the rebound time goes through a minimum as the droplet radius increases (Foote, 1975), bouncing occurs in a narrow range about $\mathrm{Cn} \sim 0.1$. This critical value increases with increasing impact parameter, at first, because the velocity normal to the droplet surfaces decreases, but this effect is overhelmed at large impact parameters by the effects of increasing droplet rotation. This rotation inhibits the flow of gas out of the intervening layer. Experimental data (Jayaratne and Mason, 1964; Brazier-Smith *et al.*, 1972) show that $s \sim 0.5$ averaged over all impact parameters in the region $0.1 \lesssim \mathrm{Cn} \lesssim 1$ with a tendency towards decreased bouncing as the droplet radius ratio decreases from unity (Levin *et al.*, 1973).

These results (see review by Abbott, 1977) are approximated here by $s = 1$ for $\mathrm{Cn} \leq 1$ and $s = 0$ (disruptive collisions) for $\mathrm{Cn} > 1$. The condition on the mean droplet radius for $s = 1$ from (28) is

$$\boxed{a < 6\sigma\rho_{\mathrm{p}}^{-1}v^{-2}.} \tag{29}$$

For coagulation, $s = 1$ for all droplets with $a > 10^{-7}$ cm for temperatures $< 10^{3}$°K (Fuchs, 1964).

3. Riming. In condensate clouds below their freezing temperature, collisions between ice particles and supercooled droplets occur. This type of coalescence is called riming. Despite the disruption of the droplets by splashing upon impact, observations in such clouds on Earth (Mason, 1971; Hobbs, 1974) suggest that enough liquid is retained and rapidly freezes on the ice particle that very efficient growth occurs. I consider $s \sim 1$ for this process.

B. Brownian Coagulation

The usual derivations of the collision rate coefficient, $R(M, M')$, for Brownian motion treat the problem as a classical diffusion problem. Chandrasekhar (1943) demonstrates the conditions under which Brownian motion is equivalent to the random walk motion of diffusion. By analogy with the diffusion of vapor, this condition is usually given as $\mathrm{Kn} \ll 1$ (e.g., Hidy and Brock, 1965a); however, the relevant length scale of the particle's motion is the stopping distance which gives $\mathrm{Stk} \ll 1$ as the proper validity condition, where Stk is evaluated with the particle's thermal velocity. This does not introduce any change in previous treatments of this problem since Stk $\sim$ Kn

when Kn $\sim$ 1 in general. I will also use the value of Kn to describe the regimes for coagulation.

A further problem of the usual diffusion analogy is the absence of any particle concentration gradient during coagulation. Fuchs (1964) avoids the use of a fictitious concentration gradient by using a probability density function instead of a physical density function. He then obtains the classical coagulation rate for a monodisperse aerosol. Generalizing to the interaction of different size particles, Fuchs (1964) gives a coagulation collision rate coefficient

$$R(M, M') = (2kT/3\eta) \times [2 + (M/M')^{1/3} + (M'/M)^{1/3}]. \quad (30)$$

When Kn $\gg$ 1 (and Stk $\gg$ 1), the interaction between the particles and the background gas is neglected and the particles are treated as a Maxwellian gas. Assuming a Maxwell–Boltzmann velocity distribution, Hidy and Brock (1965b) derive the collision rate for identical particles. They generalize to polydisperse aerosols by using a mean particle mass to calculate the thermal velocities giving

$$R(M, M') = 2(6kT/\rho_p)^{1/2}(3/4\pi\rho_p)^{1/6} \times M^{1/6}[1 + (M'/M)^{1/3}]^{-2} \times [1 + (M'/M)]^{-1/2}. \quad (31)$$

Neither the diffusion or Maxwell gas models is adequate for describing the motion of the particles in the transition regime since the background gas cannot be neglected and the particle motions are not equivalent to a random walk. Several theoretical approaches to this problem have been tried, but comparisons with the scanty and contradictory experimental data are not decisive (Fuchs, 1964; Hidy and Brock, 1965a; Fuchs and Sutugin, 1970). While the usual Cunningham correction to (30) gives good agreement with the theories and data for Kn $\leq$ 1, it is not adequate for Kn > 1. Equations (30) and (31) can be joined formally by a factor, $(1 + \text{Stk})^{-1}$, with Stk evaluated with the Stokes drag coefficient and the thermal velocity of the particles, but the meaning of this factor when Kn $\gg$ 1 is problematic.

$R(M, M')$ in (30) and (31) is a very weak function of the particle mass ratio, M'/M. Since coagulation produces a relatively narrow size distribution, the characteristic time constant for coagulation is given approximately by the value of $R(M, M')$ for the mean mass particles. With $P_1(M, M') = s = 1$ and $R(M, M') = R(\bar{M}, \bar{M})$ in (24), the time constant is

$$\boxed{\tau_{\text{coag}}^{-1} \equiv (1/N)dN/dt \approx (4kT/3\eta)N} \quad (\text{Kn} \ll 1) \quad (32)$$

and

$$\boxed{\tau_{\text{coag}}^{-1} \approx 4(3akT/\rho_p)^{1/2}N} \quad (\text{Kn} \gg 1). \quad (33)$$

These expressions compare favorably with the results of numerical calculations (Hidy, 1965; Walter, 1973) and laboratory experiments (Fuchs, 1964).

C. Gravitational Coalescence

The hydrodynamic forces on two falling particles as they approach each other change not only their trajectories but also their relative speed from its value at large distance, $V - V'$, the difference in their terminal velocities. It is convenient, however, to write the collision rate coefficient as the product of $V - V'$ and a collision cross section, $\pi E'(a + a')^2$ with the value of E' adjusted to account for any changes in the relative speed and trajectories. This adjustment is only important when $V - V'$ is small but it can require values of $E' > 1$. This formulation fails for identical particles since the nonlinear interaction of the flow fields around each particle can lead to collisions even when $V - V' = 0$. Identical particle collisions are treated as a spe-

cial case. The collision rate coefficient for coalescence is then

$$R(M, M') = (2\pi\rho_p g/9\eta)(3/4\pi\rho_p)^{4/3} \times M^{4/3}[1 + (M'/M)^{1/3}]^2 \times [1 - (M'/M)^{2/3}] \quad (\mathrm{Re} \ll 70,\ \mathrm{Kn} \ll 1),$$

$$R(M, M') = 2\pi(10\rho_p g/3\rho)^{1/2}(3/4\pi\rho_p)^{5/6} \times M^{5/6}[1 + (M'/M)^{1/3}]^2 \times [1 - (M'/M)^{1/6}] \quad (\mathrm{Re} \gg 70,\ \mathrm{Kn} \ll 1), \quad (34)$$

where $M' < M$.

The value of E' is conveniently described by three dimensionless numbers: the ratio of the particle radii, $A = a'/a = (M'/M)^{1/3} < 1$, the Reynolds number of the larger particle's motion, and the Stokes number of the smaller particle's motion near the larger particle, $\mathrm{Stk}' = \rho_p A\,\mathrm{Re}/9\rho$. This value of Stk′ is a measure of how closely the smaller particle follows the streamlines of the gas flow past the larger particle. I have used the largest velocity in Stk′ rather than the velocity difference to obtain a strict lower limit on the smallest particles for which inertial effects are important. There are several limiting cases.

1. In the limit, $\mathrm{Re} \to 0$, $\mathrm{Stk}' \to 0$, the smaller particles follow the flow streamlines which are separated from the surface of the larger particle by a distance $\delta \sim 2a/\mathrm{Re} \gg a$ in the Stokes regime (Fuchs, 1964). Thus $E' \to 0$ for all A (Davis and Sartor, 1967).

2. For intermediate values of Re, but with $\mathrm{Stk}' \ll 1$, the finite size of the smaller particles can be greater than δ and collisions can occur. This is the interception effect for which E' is still $\ll 1$ (Fuchs, 1964).

3. When $\mathrm{Re} \gg 1$, the flow streamlines are compressed towards the particles enhancing the interception effect (Fuchs, 1964). There is still a small particle cutoff since $\mathrm{Stk}' \to 0$ as $A \to 0$. This cutoff and its variation with Re have been verified experimentally (Woods and Mason, 1964; Beard and Pruppacher, 1971).

4. When $\mathrm{Stk}' \gg 1$, the motion of the smaller particle is unaffected by the gas flow around the larger particle. Thus the collision cross section is the geometric cross section, $E' \to 1$.

These general features of E' are confirmed by more detailed, but approximate, calculations (e.g., Klett and Davis, 1973; Lin and Lee, 1975; Almeida, 1977) and by experimental results (Abbott, 1977). Schlamp *et al.* (1975) show similar results for irregularly shaped particles. These results are approximated here by $E' = 0$ when $\mathrm{Stk}' < 1$ and $E' = 1$ when $\mathrm{Stk}' > 1$.

The calculation of the interaction of two identical particles requires precise knowledge of the flow fields around both particles. For $\mathrm{Re} \to 0$ and separation distances greater than the gas mean free path, analytic solutions of this problem show that no collisions occur (Davis and Sartor, 1967). Early approximate solutions for higher Re indicated a negligibly small value of E', but these calculations neglected the interaction of the upper particle with the wake formed downstream of the lower particle. Careful, low turbulence laboratory experiments produce collisions for initial separations as large as 100 particle radii (Spengler and Gokhale, 1973; Abbott, 1974). Later calculations of E' also found similar results (e.g., Klett and Davis, 1973; Lin and Lee, 1975). Since the actual environment of aerosols is more turbulent than either the theoretical or the experimental conditions, the small random motions of the particles produced by the turbulence cannot be neglected when $V - V' \approx 0$. These motions not only ruin the precise, long-term alignment of the particle trajectories required for wake capture but also lead to collisions between identical particles in shorter times. The wake capture process is not expected

to be important in realistic circumstances (Berry and Reinhardt, 1974).

The interaction of colliding spheres when Kn > 1 has not been investigated, although Davis (1972) and Dahneke (1973) extend the theory for Kn $\ll$ 1 up to Kn $\sim$ 1 with a Cunningham factor. Qualitatively though, the influence of the gas on the particle trajectories must decrease as the gas density decreases. Thus $E' \to 1$ for all A when Kn $\gg$ 1.

The factors involving the mass ratio in (34) are nearly constant for mass ratios $<10^{-1}$ and go rapidly to zero for mass ratios >0.5. The value of E' goes rapidly to zero for mass ratios $<10^{-1}$ (Woods and Mason, 1967; Beard and Pruppacher, 1971). Therefore, the coalescence time constant is given approximately by $R(M, M') = R(\bar{M}, 0.5\bar{M})$:

$$\boxed{\tau_{\text{coal}}^{-1} \approx (\pi \rho_p g/9\eta) a^4 N} \quad (\text{Re} \ll 70,\ \text{Kn} \ll 1), \quad (35)$$

$$\boxed{\tau_{\text{coal}}^{-1} \approx (10\pi^2 \rho_p g a^5/3\rho)^{1/2} N} \quad (\text{Re} \gg 70,\ \text{Kn} \ll 1), \quad (36)$$

$$\boxed{\tau_{\text{coal}}^{-1} \approx (4\pi \rho_p g/27\rho)(\pi m/2kT)^{1/2} a^3 N} \quad (\text{Kn} \gg 1). \quad (37)$$

Berry and Reinhardt (1974) derive an effective mass ratio of roughly $\frac{2}{3}$ instead of $\frac{1}{2}$ from detailed numerical calculations. These equations apply to the size range of particles in which $s \approx E' \approx 1$.

D. Summary and Comments

Most of the uncertainty in estimating τ_{coag} and τ_{coal} is in the determination of the values of s and E'.

1. For coagulation, $s = 1$ for all particles with $a > 10^{-7}$ cm. No disruptive collisions occur.

2. The smallest particle size for which coalescence is efficient is determined by the hydrodynamic limits on E'. This limit is determined by the condition Stk > 1.

3. The largest particle size for which coalescence growth occurs is determined by the onset of disruptive collisions.

4. For solid particles resembling dust grains, coalescence growth does not occur, since only bouncing occurs in the size range for which $E' \approx 1$. For ice and liquid droplets, coalescence growth is efficient for the whole size range for which $E' \approx 1$ up to the disruptive collision size limit.

There are two phenomena which are not of primary importance in themselves but which modify the efficiency of coalescence significantly. The first phenomenon is turbulence. Theoretical estimates of the particle collision rate caused by turbulence indicate that this process is always less important than coalescence in natural aerosols (e.g., Saffman and Turner, 1956; Fuchs, 1964; Jonas and Goldsmith, 1972; Tennekes and Woods, 1973). However, the additional relative velocity of the particles produced by turbulence, while causing no significant increase in the collision rate, does increase the value of E' and broaden the particle size range over which efficient coalescence growth occurs (Almeida, 1977). This lowering of the hydrodynamic limit on collisions is crudely represented by using the larger particle's terminal velocity to determine Stk′.

The second phenomenon is the action of electrostatic forces between charged aerosol particles. There are two effects. The first is an increase in the particle binding energies which decreases the particle size range over which bouncing occurs. While this effect on s is not that significant for the coalescence growth of ice and liquid droplets, it can drastically increase the coalescence growth efficiency in dust grain clouds. The second effect is an increase in the relative velocities of the particle collisions. This not only makes the hy-

drodynamic limits on collisions less important, but also results in values of $E' \gg 1$ (Schlamp *et al.*, 1976). Thus the coalescence growth efficiency of charged aerosols can be much greater than estimated here. Without information about electric charges on aerosols in other atmospheres, I cannot determine the importance of their effects on my conclusions.

VI. THE CLOUDS OF EARTH

A description of the clouds in Earth's atmosphere for which the cloud microphysical theories were developed is a natural complement to the brief summary of these theories in the preceding three sections, but that description in this section also has two other purposes. The first purpose is to describe the analysis method to be applied to the clouds in other atmospheres by applying it to the most familiar clouds. The method of comparing the estimated time constants of the primary microphysical processes is systematic, but also qualitative, and the application of this method first to reasonably well understood clouds illustrates both its validity and its limitations. The second purpose is to describe, more precisely, the cloud models to be used to form analogies with clouds in other atmospheres. The description consists of the most important properties of the cloud and atmosphere and their significance in the determination of the principal processes producing the cloud.

Each subsection in this and the next section is organized in three parts. First there is a very brief summary of the observed cloud and atmospheric properties required for the analysis. These are the cloud composition, location, mass density and mean particle radius (defined by the mean particle mass), and the atmospheric composition, density, and temperature. In general, the cloud composition, location, and mass density, together with the atmospheric properties, determine whether the cloud is a condensate cloud or a dust cloud, but the choice between a cooling cloud and a chemical cloud is not as easy. In the case of water clouds on Earth, the summary of properties is far from complete and is only an overview of typical cloud properties and atmospheric conditions equivalent to the type of information available for the other planets. At the opposite extreme is the Jovian ammonia–water cloud which has not been observed at all.

In the second part of each subsection, the time constants, τ_{cond}, τ_{fall}, τ_{coag}, and τ_{coal}, are compared to each other in a diagram (cf. Fig. 2) to determine the dominant processes operative in each cloud system. The equations enclosed in boxes in the text show that the time constants are most sensitive to the values of the cloud particle number density, the cloud particle mean radius and the atmospheric mass density. The diagram shows the dependence of the time constants on the particle radius at a fixed atmosphere density in a constant mass cloud in which $N \propto a^{-3}$. There are several important features of this type of diagram.

(a) Since collisional growth processes conserve the total mass, the curves representing τ_{coag} and τ_{coal} are approximate evolutionary tracks for the mean particle radius of a constant mass cloud.

(b) The curve for τ_{cond} is not an evolutionary track since τ_{cond} is not a function of particle number density and condensation does not conserve total mass. Instead this curve simply represents the growth time as a function of particle size. Since the largest particles grow most slowly, each point on τ_{cond} also represents the approximate time required by a cloud to attain a particular mean particle size. There is not a straightforward dependence of τ_{cond} on the cloud mass density, although more massive clouds may be associated with higher values of ρ_s.

(c) As a consequence of (a) and (b),

a change in the cloud mass density shifts the positions of τ_{coag} and τ_{coal} relative to τ_{cond} and τ_{fall}. It is these relative positions that determine the different cloud types.

The third part of each subsection is a discussion of the interpretation of the first type of diagram. In the case of water clouds on Earth, these interpretations are compared to more detailed observations and better theoretical results to determine the validity of the diagrams. For other clouds, the interpretations are compared to those for more familiar Earth clouds to determine, in a systematic way, the proper analogies between Earth and other planetary clouds. The interpretations are summarized in a second type of diagram (e.g., Fig. 4) which shows, schematically, the dominant microphysical process in each atmosphere as a function of cloud particle radius and atmospheric density for the appropriate cloud density.

In this section, I discuss three cloud or aerosol systems in Earth's atmosphere which are the models for other planetary clouds. These systems are, in order of decreasing knowledge, (i) the tropospheric water clouds which are the model for cooling clouds, (ii) the stratospheric sulfuric acid cloud which is one model for chemical clouds, and (iii) the tropospheric aerosols, or CCN, which include both a chemical cloud component and a dust cloud component.

A. Tropospheric Water Clouds

The water clouds in Earth's lower atmosphere (below ≈ 15 km) are the densest, and therefore, the most important aerosols. The mass mixing ratio of the clouds is so high (from $\sim 10^{-4}$ to $\sim 10^{-3}$) that they significantly alter the atmospheric radiation balance (high visual albedo and low infrared albedo), dynamics (high latent heat of condensation), and vertical transport of other gases and aerosols (efficient washout by falling water droplets). Most of these clouds form in updrafts associated either with small-scale ($\sim$1–10-km) convective motions (cumulus clouds) or with large-scale ($\sim$100–1000-km) dynamic systems (stratus clouds) with roughly half of Earth covered by clouds on average. Typically, these clouds attain their full mass density in a time $\sim 10^3$ to $\sim 10^4$ sec. The lifetime of individual cumulus clouds varies from $\sim 10^3$ to $\sim 2 \times 10^4$ sec, with the larger lifetimes associated with stronger weather systems (Mason, 1971). The cloudiness associated with large-scale weather systems (both cumulus and stratus) has a lifetime comparable to that of the system itself, $\sim 10^4$ to $\sim 3 \times 10^5$ sec.

The most important properties of water clouds in the lower troposphere, below ≈ 5 km, are as follows (Fletcher, 1962, Mason, 1971, Hobbs, 1974).

1. The phase of water in these clouds varies with location and season, but for most of the year over most latitudes the "typical" low altitude cloud is a liquid water cloud.

2. If a just saturated volume of air were cooled by uplift, the mass density of the condensed cloud would be equal to $\rho_v - \rho_s$, the adiabatic cloud mass content. However, since Earth's atmosphere is normally undersaturated and ascending air parcels continually mix with the drier surrounding air, the actual cloud mass content rarely attains its adiabatic value, except locally within a cloud. The observed range of the mean cloud mass density is from $\sim$0.1–1.0 g m^{-3}, $<$0.1 the adiabatic value for small cumulus clouds, to $\sim$3 g m^{-3}, $\sim$0.3 the adiabatic value for large cumulus clouds. Stratus clouds cover a similar range of mass densities.

3. The most fundamental property of water clouds is the presence or absence of precipitation (see Fig. 1) which depends most strongly on the cloud mass density. The lower limit for precipitation is $\sim$1 g m^{-3} (Mason, 1971). All other cloud prop-

erties vary strongly between nonprecipitating and precipitating clouds.

4. The vertical extent of these clouds, is smaller than an atmospheric scale height with the exception of massive, precipitating clouds which have vertical extents approaching a scale height. Precipitating clouds are also massive enough that the latent heat released by their formation causes stronger than normal updrafts.

5. The number density of cloud particles is controlled by the CCN number density (Twomey, 1977) and ranges from $N \sim 50$ cm^{-3} for maritime clouds to $N \sim 200$ cm^{-3} for continental clouds. Consequently, the mean particle radius varies slightly between these two types of clouds. Maritime clouds are also more likely to produce precipitation than equal mass continental clouds. For nonprecipitating clouds, the mean radius is typically $\bar{a} \lesssim 10$ μm with a narrow size distribution, somewhat broader than that caused by condensation alone. For precipitating clouds, $\bar{a} \gtrsim 30$ μm with a very broad, even bimodal size distribution (Warner, 1969; Mason, 1971). The mean size of precipitation is $\bar{a} \sim 200$ to 500 μm with a very broad size distribution which is broader for larger precipitation rates (Marshall and Palmer, 1948; Mason, 1971).

The most important properties of upper tropospheric clouds (above ≈ 5 km) are as follows (Fletcher, 1962; Mason, 1977; Hobbs, 1974; Twomey, 1977).

1. The mixing ratio of total water decreases with altitude in Earth's atmosphere, and consequently, the mass density of upper tropospheric clouds is typically one to two orders of magnitude smaller than that of lower tropospheric clouds, ~ 0.1 to 50×10^{-2} g m^{-3}.

2. High-altitude (cirrus) clouds are composed of water ice.

3. The particle number density of cirrus clouds is generally much smaller than that of lower-altitude clouds, $N \sim 1$ to 10 cm^{-3}, but the mean particle radius is much larger, $\bar{a} \gtrsim 50$ to 100 μm. Little is known about the size distributions.

4. Two common features of ice clouds are the diffuse outline and presence of fall streaks below the cloud. Both of these features are a consequence of the nucleation of ice as supercooled liquid droplets that freeze (Twomey, 1977). This means that the cloud does not form until liquid water saturation is attained, well above the ice saturation level. Thus, ice particles transported or falling out of the cloud remain in ice supersaturated conditions and even continue to grow. The sharp outline of liquid water clouds occurs because the surrounding air is not water saturated and the droplets evaporate when removed from the cloud.

Figure 2a shows the time constants for a low-altitude (~ 0 km), liquid water cloud with a mass density, $\mu = 2 \times 10^{-3}\rho = 2$ g m^{-3}, typical of a massive cumulus cloud. If Earth were observed from space, several facts would strongly suggest that the water clouds are cooling clouds condensing on CCN: (i) The large amount of water on the surface (the ocean) and in the atmosphere eliminates the need for a "chemical" source of water; (ii) the atmospheric temperature structure and the water vapor abundance create nearly saturated conditions in the lower atmosphere; and (iii) the number density of smaller aerosols ($\bar{a} \lesssim 1$ μm) is much larger than the typical number density of water cloud particles. Figure 2a clearly confirms this suggestion by demonstrating that condensation, even at the low supersaturations characteristic of condensation on CCN, is the only growth process fast enough to produce 10 μm droplets, or larger, in a time $\sim 10^3$ to $\sim 10^4$ sec, as observed on Earth. Coagulation is much too slow and coalescence is ineffective for particles with $\bar{a} \lesssim 10$ μm.

Figure 2a also provides a fundamental

understanding of precipitation and its formation. Precipitation is important because it transports water so rapidly to the surface of Earth that the atmosphere remains undersaturated on average even in the presence of the ocean and turbulent mixing in the lower atmosphere. This significant downward transport of water can only occur if $\tau_{evap} > \tau_{fall}$ for the particles; hence, large particles and precipitation particles are distinguished from small cloud particles by this property in Fig. 1. Figure 2a shows that the only process that can produce such particles is coalescence, i.e., $\tau_{growth} = \tau_{coal}$ in Fig. 1. The maximum mean particle radius produced by coagulation or condensation is limited by sedimentation so that even a modest undersaturation below the cloud, $S \sim (-10^{-2})$ say, is sufficient to give $\tau_{evap} \ll \tau_{fall}$ for particles with $\tau_{coag} \sim \tau_{fall}$ or $\tau_{cond} \sim \tau_{fall}$.

The reason for a critical cloud mass density for the onset of precipitation is now clear. Since the droplet number density is fixed by the CCN number density in the updraft, the cloud mass density is equivalent to a mean particle radius which must exceed the lower size limit on efficient coalescence set by hydrodynamic effects, the Stokes number condition. Thus, the decrease in cloud particle mean size caused by a larger CCN number density inhibits precipitation even when the cloud

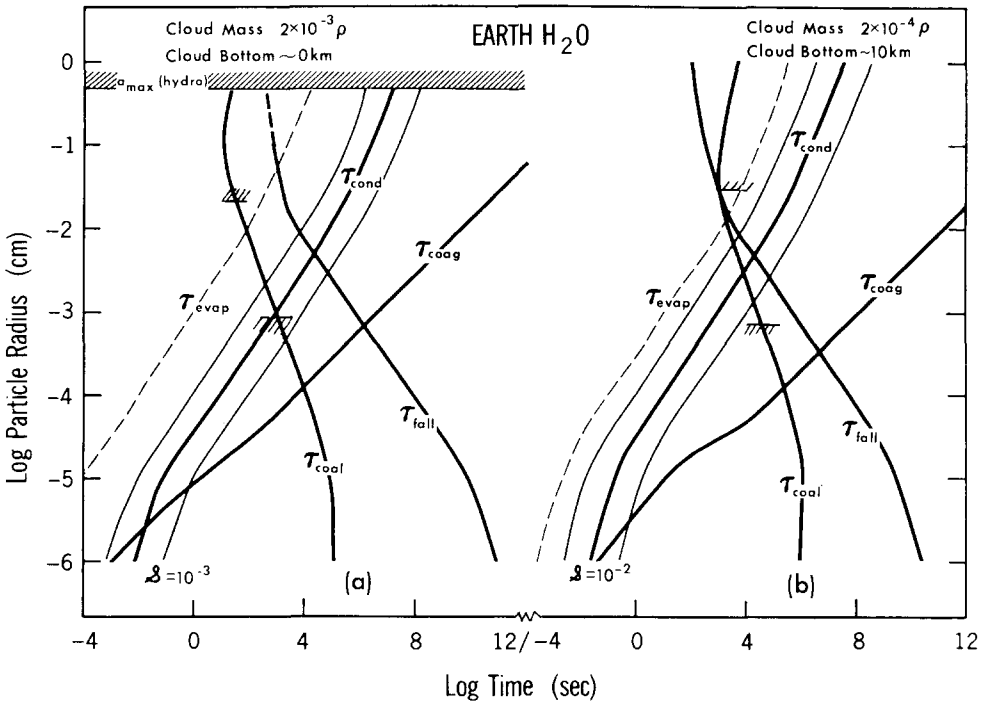

FIG. 2. Microphysical time constants as a function of mean particle radius in constant mass clouds for (a) Earth water clouds and (b) water ice clouds. The three τ_{cond} curves represent the growth time for supersaturations one order of magnitude smaller and larger than the value indicated. The τ_{evap} curve is a lower limit since it is calculated assuming $\rho_v = 0$. The lower hash mark on the τ_{coal} curve represent the Stokes number condition for efficient particle collisions and the upper hash mark represents the particle radius above which collisions are disruptive. For liquid droplets, the τ_{fall} curve is dashed when the Weber number exceeds unity and the hydrodynamic upper limit on the radius is indicated by a_{max}(hydro).

mass density is large enough, as in continental clouds compared to maritime clouds. Since there is no way to calculate the cloud particle number density, Fig. 2a cannot be used to predict precipitation in individual clouds, but it does show, correctly, that Earth clouds do attain the required mass density and mean particle radius in their lifetime to produce precipitation.

Once initiated, coalescence rapidly increases the mean particle radius in the cloud until, as Fig. 2a shows, it is limited by disruptive collisions. Although this limit does not depend on the precipitation rate as observed, it is qualitatively correct. Furthermore, the precipitation particles larger than the mean size have $\tau_{evap} \gtrsim \tau_{fall}$, i.e., these particles ($a > 100$ μm) have no trouble reaching Earth's surface from low-altitude clouds.

Figure 2b shows the time constants for a high-altitude ($\sim$10 km) water ice cloud, or cirrus cloud, with a mass density, $\mu = 2 \times 10^{-4}\rho = 8 \times 10^{-2}$ g m^{-3}. The short formation time ($\lesssim 10^4$ sec) and the large mean particle size of cirrus clouds is only consistant with condensation growth as the primary formation process. Furthermore, the diffuse outline of these clouds and the temperatures at which they form suggest that nucleation occurs at water saturation. Consequently, the condensation growth time of particles with $a > 10$ μm is much shorter than in lower-altitude clouds.

There is a critical cloud mass density required for precipitation to form in these clouds; but, as Fig. 2b shows, because of the rapid condensation growth rate, it is not the Stokes condition that inhibits coalescence. Instead, the mass density is so low that $\tau_{coal} \sim \tau_{fall}$ when $\tau_{cond} > \tau_{coal}$. Consequently, coalescence growth in less massive clouds is slower than the sedimentation removal of the particles (cf. Fig. 1). The critical mass density is further increased by the small vertical extent of the clouds which decreases the effective value of τ_{fall} and by turbulent dispersal of the cloud. Therefore, only the most massive cirrus clouds, with mass densities exceeding $\sim$0.1 g m^{-3}, produce snow.

In contrast to lower-atmosphere clouds, the growth of precipitation in these clouds is limited by sedimentation rather than by disruptive collisions. This is caused not only by the small vertical extent of the clouds but also by the inefficiency of disruptive collisions in limiting the growth of snow (cf. discussion in Section V, Part A). Even though the precipitation produced by these clouds falls a substantial distance under ice supersaturated conditions, the extremely low terminal velocity of the porous snow particles usually precludes their reaching the surface before evaporating. However, these ice and snow particles often stimulate precipitation in lower, supercooled clouds (Wexler, 1960; Mason, 1971).

The effects which have been neglected in this very simple analysis do not significantly change the interpretation of Fig. 2.

1. A condensation coefficient, $\alpha \ll 1$, shifts the "kink" in the τ_{cond} curve in Fig. 2 towards a larger particle radius. However, even the smallest reported values of $\alpha \sim 10^{-2}$ for liquid water (Warner, 1969) do not significantly increase the growth time of droplets with $\alpha \gtrsim 10$ μm. The value of $\alpha \sim 10^{-3}$ for water ice (Choularton and Latham, 1977) does retard the growth of ice crystals with $\alpha \lesssim 100$ μm, but this is more than compensated for by the high supersaturation of liquid nucleation at these altitudes, $\sim 10^{-1}$.

2. The Bergeron growth process, with effective supersaturations $\sim 10^{-1}$, accelerates the formation of precipitation to times as short as $\sim 10^3$ sec by producing many very large particles (Wexler, 1960; Mason, 1971; Hobbs, 1974). Seeding the upper

portions of a supercooled liquid water cloud with ice crystals often stimulates further droplet freezing leading to Bergeron growth and precipitation. However, the possibility of growth occurring by this process does not alter the conclusion that precipitation is formed by sufficiently massive water clouds.

3. Numerical investigations (Sutugin and Fuchs, 1970; Pich *et al.*, 1970; Jonas and Mason, 1974; K. C. Young, 1975; Hamill *et al.*, 1977) show that the simultaneous operation of all the aerosol processes hastens the transition from the dominance of one process to another. An especially important example of this effect is the acceleration of coalescence by continued condensation and turbulence (Jonas and Mason, 1974). Thus the growth time of the cloud and the time required to produce precipitation shown in Fig. 2 are somewhat large, but still correct within an order of magnitude.

Since the coupling between the microphysics and the dynamics is not considered, Fig. 2 cannot determine the detailed properties of clouds and their evolution, especially precipitation clouds on Earth. However, this diagram, together with observations of cloud mass density and mean particle size, does correctly identify the dominant processes operative in the cloud and the trend of subsequent development, in this case, the formation of precipitation.

B. Stratospheric Sulfuric Acid Cloud

The bulk of the aerosol layer in the stratosphere between ~15 and 30 km is composed of sulfuric acid–water solution droplets containing some ammonium sulfate [see Junge (1963), Castleman (1974), Cadle and Grams (1975), and Toon and Pollack (1976), for reviews]. The large natural variability of this aerosol in time and space, together with the formidable experimental problems associated with detecting submicron particles reliably, leads to a wide variety of estimates of its typical properties.

1. The abundance of water vapor in the stratosphere ($\sim 3 \times 10^{-6}\rho$) is consistent with vapor equilibrium over 75% concentration sulfuric acid solution droplets, but suggests that these droplets evaporate above ~35 km (Hamill *et al.*, 1977). The sulfuric acid vapor abundance has not been measured.

2. The cloud mass density is a maximum near 20 km. Although the total aerosol number density is a minimum there, the sulfuric acid droplet number density is a maximum. This strongly suggests that condensation occurs in this region.

3. Typical values of the mass density and number density are $\sim 2 \times 10^{-9}\rho = 2 \times 10^{-7}$ g m^{-3} and ~1 cm^{-3}, respectively. These values are somewhat larger than the average background cloud densities, but much smaller than the peak values attained after a large volcanic eruption or nuclear explosion (Castleman, 1974). The corresponding mean particle radius is $\bar{a} \sim 0.5$ μm.

4. The estimated number density of other particles ($\bar{a} < 0.1$ μm) mixed up from the troposphere is $N > 10$ cm^{-3}.

5. After a major volcanic eruption or nuclear explosion, the sulfuric acid cloud mass density increases sharply. The lag time between the injection event and the peak mass density is $\sim 3 \times 10^7$ sec. The lifetime in the stratosphere of the submicron particles from these events is $\sim 10^8$ sec (Castleman, 1974), while their lifetime in the troposphere is $< 10^6$ sec because of rainfall activity.

Studies of the isotopic sulfur composition of collected samples of stratospheric aerosols after major volcanic eruptions point to in situ chemical reactions as the source of the sulfuric acid vapor that condenses into the droplets (Castleman, 1974); hence this cloud is the prototype

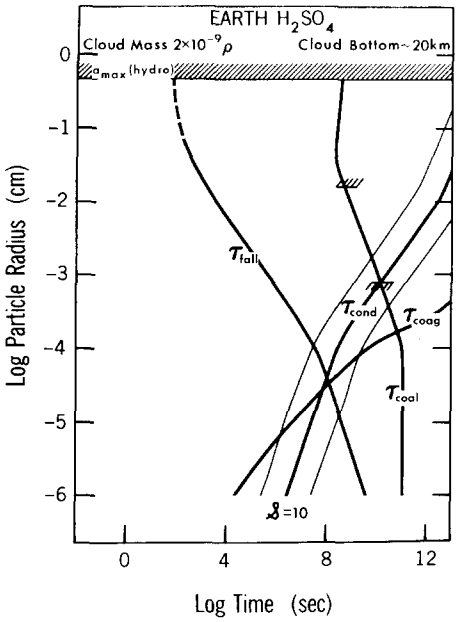

FIG. 3. Same as Fig. 2 for Earth sulfuric acid clouds.

chemical cloud. Figure 3 shows the time constants for this cloud at 20 km with $\mu = 2 \times 10^{-9}\rho$. Since the particles appear in a time $<3 \times 10^7$ sec and the values of τ_{cond} for $\mathcal{S} \sim 10^{-3}$ is $\gg 10^8$ sec, the chemical reactions are clearly rapid enough to increase the supersaturation to much higher values. The larger value of $\mathcal{S}$ for effective growth is also required because sulfuric acid is involatile at these temperatures (cf. Section III, Part A7). If the cloud is in a steady state, then the cloud particle size is limited by $\tau_{cond}^{-1} = \tau_{remove}^{-1}$. For the purpose of discussion, $\rho_s\mathcal{S}$ has been adjusted to meet this condition for 0.5-μm particles. For $\rho_s \sim 10^{-14}\rho$ (Hamill *et al.*, 1977), the supersaturation is ~ 10 (if $\alpha = 1$).

Figure 3 makes two facts immediately clear. First the observed particle lifetime in the stratosphere is consistent with $\tau_{remove} = \tau_{fall}$, with only a weak contribution by turbulence possible, but this may not be true for all locations and seasons. Second, the sulfuric acid cloud is so tenuous that coalescence plays no role in shaping its microstructure; no precipitation is formed. However, since sulfuric acid is involatile even in the troposphere, the particles falling out of the stratosphere do not readily evaporate. They behave more like dust.

Figure 3 shows that there are two possible explanations of the growth of the sulfuric acid droplets from the vapor. The key to the choice between them in the nature of the embryos produced by the gas phase chemistry. The theory of heterogeneous nucleation of a vapor, discussed in Section III and used by Hamill *et al.* (1977) in their condensation model of this cloud, starts with a Boltzmann distribution of vapor molecule aggregates on the surface of background aerosol particles which is only established after a sufficient number of vapor molecule collisions occurs. This presents no problem unless the sulfuric acid molecules first encounter other molecules with which they react chemically. In this case, the presence of $\sim 10^4$ water molecules for every sulfuric acid molecule means that each sulfuric acid molecule suffers many collisions with water molecules and becomes completely hydrated (Friend *et al.*, 1973) before encountering another sulfuric acid molecule. Now if the hydrated sulfuric acid aggregate behaves like a large vapor molecule of sulfuric acid–water solution, then subsequent collisions produce no net growth but do establish a statistical distribution of larger aggregates. These, in turn, can become actively growing droplets when the supersaturation of the "solution vapor" grows large enough. The hydrated sulfuric acid aggregates themselves cannot act as embryos for condensing sulfuric acid molecules because newly produced sulfuric acid molecules are incorporated into a new aggregate before they collide with any old aggregates. If, however, the aggregates behave like small particles then collisions with each other produce net growth even

when the "supersaturation" is low or negative, i.e., coagulation occurs.

The only observations that might distinguish between these two growth models are extremely difficult to make and difficult to interpret in the absence of any knowledge of the properties of large molecular aggregates. For instance, a measurement of the sulfuric acid vapor density is not decisive if the proper value of ρ_s is unknown. If the cloud particle growth is limited by particle removal as assumed here, then a measurement of the particle size distribution and composition below 0.1 μm in radius might reveal whether the cloud particles begin their growth as moleculer size aggregates or larger, background aerosol particles. Unfortunately, there is evidence that the sulfur inputs to the stratosphere vary on a time scale $<3 \times 10^7$ sec (e.g. Castleman, 1974), which, as Fig. 3 suggests is shorter than the relaxation time of this cloud, $>3 \times 10^7$ sec. If observations reveal that the sulfuric acid droplets complete their full growth in a time $<3 \times 10^7$ sec and that their number density is <1 cm^{-3}, then coagulation is too slow to explain this behavior. It is possible that the "typical" cloud properties are misleading. Neither of these explanations of the sulfuric acid particle growth can be ruled out as yet. This problem shows the importance of good observations for determining the correct microphysics of a cloud and is an outstanding illustration of the importance of all the poorly understood processes, here collected under the label "chemical nucleation."

C. Other Tropospheric Aerosols

The "dirt" in Earth's "dirty" atmosphere, the CCN, is an extremely complex aerosol containing particles from many different sources, of many different compositions, and of all sizes. (See reviews by Junge, 1963; Toon and Pollack, 1976). This dirt has many important effects on both of the cloud systems discussed in Parts A and B, the two most important being the control of the critical water cloud mass density required for precipitation, and the control of the particle number density in the stratospheric sulfuric acid cloud if condensation growth predominates. Systematic investigations of this aerosol system have only recently begun. I include this brief section to emphasize the importance of these particles and the rudimentary understanding of the processes that control them.

Roughly half the mass of the tropospheric aerosols is particles in the radius range, 0.1 μm $< a <$ 1.0 μm, composed largely of sulfate compounds and formed almost entirely by chemical reactions (Junge, 1963; Vohra and Nair, 1970; Cadle and Grams, 1975). These particles are another example of a chemical cloud. Some studies of the microphysics of this cloud have been completed (Brock, 1972; Husar *et al.*, 1972). The growth process appears quite complicated: Chemical reactions form particles large enough for efficient coagulation up to Aitken sizes ($\bar{a} \lesssim 1.0$ μm) where condensation of water and other chemically produced vapors becomes the predominant growth process up to the observed size range. Almost all of the rest of the aerosol mass is windblown surface soil with radii, 1.0 μm $< a <$ 10 μm. The study of these particles has focused primarily on the interaction of turbulent atmospheric motions with the planetary surface (Bagnold, 1941; Chepil and Woodruff, 1963; Gillette *et al.*, 1974; Iversen *et al.*, 1976), but not on the microphysics of the airborne cloud. This aerosol, especially in the form of localized dust storms, is an analog for windblown aerosols on other planets.

D. Summary and Comments

Figure 4 summarizes the discussion of the tropospheric water clouds and the

stratospheric sulfuric acid cloud by showing the predominant microphysical process for each particle size range. The observed mean particle radius is indicated by the hatched region. This is not shown for the very large range of particle sizes in water clouds. These two clouds are the prototype cooling and chemical cloud models, respectively, for comparison with clouds in other atmospheres.

I have shown in this section that when adequate information about a cloud exists, the time constant diagrams can correctly identify the primary microphysical processes at work in the cloud. These diagrams do not accurately describe the evolution of clouds, only the qualitative trends. Further, when adequate information about a cloud does not exist, as for other planetary atmospheres, these diagrams clearly define the alternative models for the cloud structure and evolution.

VII. THE CLOUDS OF VENUS, MARS, AND JUPITER

A. The Clouds of Venus

Recent ground-based and spacecraft observations of the planet-wide cloud cover suggest that above $\sim$60 km it is a complex aerosol system of several overlapping, possibly interacting, haze layers with properties that vary with time and location [cf. the special June 1975 issue of *J. Atmos. Sci.* **32**, especially O'Leary (1975), Martonchik and Beer (1975), A. T. Young (1975), and Hapke (1976), Keldysh (1977), and A. T. Young (1977)]. Most of the available data apply to the sulfuric acid–water cloud which is the dominant component of the cloud that is visible from outside the atmosphere. I consider only this cloud here.

1. The cloud particles in the atmosphere above $\approx$60 km are $\approx$85% sulfuric acid by mass (Pollack *et al.*, 1978). At the temperatures in this part of the atmosphere ($\lesssim$300°K), the vapor in equilibrium with such particles is entirely water. At the high temperatures in the lower atmosphere, these particles evaporate.

2. Since the water vapor abundance varies strongly with time and location (Young, 1975) and, in particular, it is not uniformly mixed with altitude (Pollack *et al.*, 1978), estimates of its abundance are difficult to make. The range of estimated mixing ratios (10^{-6}–10^{-3}) suggests that water is primarily in vapor form, rather than in the sulfuric acid particles, and more abundant than sulfuric acid. Thus, the acid concentration of the cloud particles is determined by the local water abundance rather than the reverse (Pollack *et al.*, 1978).

3. The cloud mass mixing ratio above 60 km decreases with altitude (Lacis, 1975). This means that the source of cloud particles must lie at or below this level since such a mass distribution only occurs when upward turbulent transport opposes sedimentation above a source region (Rossow, 1977). The lifetime of particles at this altitude is, therefore, not much longer than τ_{fall}. More recent Earth-based infrared observations (Pollack *et al.*, 1978) and the nephelometer experiments on the Venera 9 and 10 entry probes (Keldysh, 1977) indicate that the cloud mass mixing ratio increases with depth down to $\sim$50 km.

4. Upward looking photometers on Venera 8 (Marov *et al.*, 1973) and on Venera 9 and 10 (Keldysh, 1977) detected a cloud bottom at 35 and 50 km, respectively. Since the measured temperature difference ($\sim$20°K) and even an order of magnitude change in the water abundance cannot explain such a large change in the cloud particle evaporation level (Wolfsy, 1974), these observations remain unexplained.

5. Assuming a constant mixing ratio of total water and sulfuric acid, Rossow and Sagan (1975) find an upper limit on the cloud mass density, $\mu < 10^{-5}\rho$, consistent with the available data. Relaxing this as-

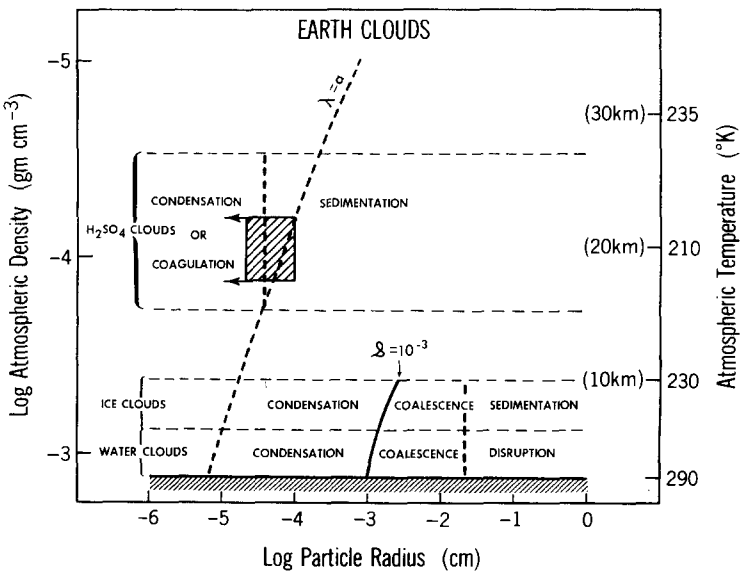

FIG. 4. Regime diagram for Earth clouds showing dominant microphysical process as a function of atmospheric density and mean cloud particle radius. Hatched regions indicate observed mean particle radii.

sumption, Pollack *et al.* (1978) find $\mu \sim 6 \times 10^{-6}\rho$ averaged over the cloud.

6. From the polarization of sunlight reflected by the clouds, Hansen and Hovenier (1974) find that the cloud particles are spherical, i.e., liquid droplets, with a mean radius ~ 1 μm. The droplet number density at 70 km is $N \sim 10^2$ cm^{-3} and the size distribution is somewhat narrower than is typical of water clouds but similar in width to the stratospheric haze layer on Earth. The nephelometer results from Venera 9 and 10 show a increase of the droplet mean radius to ~ 2 μm and a slight decrease of their number density with depth to 50 km (Keldysh, 1977).

7. The observed cloud lifetime, $> 10^9$ sec, suggests that, to first order, the cloud is in a steady state.

There are two models for the chemical behavior of sulfuric acid in Venus' atmosphere. Sulfuric acid partially decomposes, during evaporation, into water and sulfur trioxide, a very reactive gas. Prinn (1973) argues that the sulfur trioxide is irreversibly destroyed in a reducing lower atmosphere by reaction with such gases as carbon monoxide. He, therefore, proposes that the sulfuric acid is reformed photochemically near the cloud top in analogy with the stratospheric sulfuric acid cloud on Earth. Figure 5 shows the time constants for this cloud model at 60 km with $\mu = 10^{-5}\rho = 5 \times 10^{-3}$ g m^{-3}. For a steady state cloud, $\rho_s \mathcal{S}$ is adjusted to give $\tau_{cond} \sim \tau_{fall}$ for 1-μm droplets, where $\rho_s \sim 10^{-11}\rho$ and $\mathcal{S} \sim 1$ for 75% sulfuric acid (Hamill *et al.*, 1977). (For 85% sulfuric acid $\rho_s \sim 2 \times 10^{-10}\rho$, $\mathcal{S} \sim 0.05$.) The vertical extent of the formation region near 60 km is probably ~ 6 km, the atmospheric density scale height. It cannot be any deeper because the needed photons do not penetrate any deeper. On the other hand, if the sulfur trioxide and sulfuric acid are not destroyed in an oxidizing lower atmosphere, then the cloud droplets reform from the vapor at the cloud bottom in analogy with the photochemical smogs in Earth's troposphere. Figure 6 shows

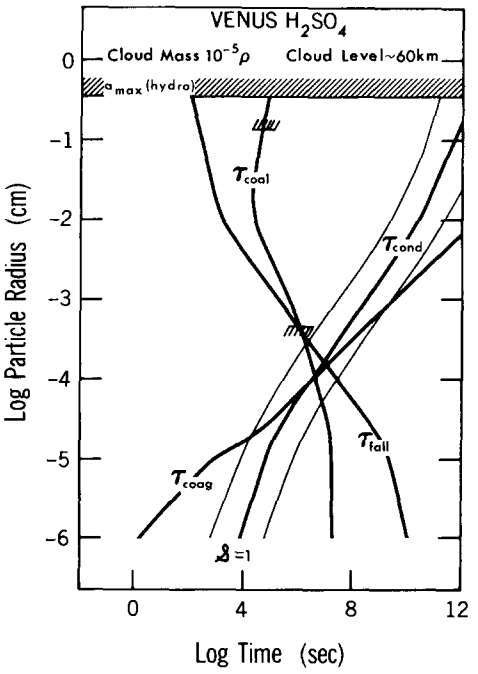

FIG. 5. Same as Fig. 2 for Venus sulfuric acid droplet clouds, photochemical model.

the time constants for this cloud model at 30 and 50 km with the same cloud mass mixing ratio. If sulfuric acid vapor condenses at these high temperatures like water vapor, then ρ_s would be $\sim 10^{-5}\rho$ and $S \sim 10^{-3}$ as shown. The vertical extent of this formation region is also small since the temperature lapse rate is large, $\sim 8°K\ km^{-1}$ (Marov, 1972) and chemical reaction rates or saturation vapor densities are exponentially dependent on temperature.

In the main part of the cloud, outside of the droplet formation and evaporation regions, the fact that the droplets are almost entirely sulfuric acid and the vapor is entirely water means that the composition effect on the equilibrium vapor density, S_{CCN} in (8), completely overwhelms the droplet size effect, S_{curv}, preventing any vapor exchange between different size droplets. Although the droplets adjust composition in response to changing water abundance, the water vapor density is much smaller than saturation for pure water droplets. Consequently, the particles are condensationally inactive like the CCN in Earth's troposphere at extremely low humidities. Figures 5 and 6 also show that coalescence of 1-μm droplets is prevented by the hydrodynamic forces on them and no precipitation is formed in these clouds. The only effective microphysical process in the main part of the cloud on a time scale $< \tau_{fall}$ is coagulation, a conclusion independent of the formation process.

Figure 5 shows that the analogy between the Venus sulfuric acid haze and Earth's stratospheric haze suggested by Prinn (1973), extends to the uncertainty in determining the dominant growth process. If the cloud is in a steady state so that droplet growth is limited by sedimentation, then the observed mean droplet radius is consistent with either condensation or coagulation in the final growth stage. In contrast to the situation with Earth's stratospheric haze, the much larger mean droplet radius in this cloud makes the size distribution below the mean more accessible to observation. If the sulfuric acid vapor were converted to small particles by chemical reactions (there may be enough water to hydrate the sulfuric acid molecules), with subsequent coagulation growth, then the steady state size distribution would contain numerous droplets smaller than the mean size. In a numerical investigation of this case (Rossow, 1977), I show that the droplet size distribution produced by the coagulation of submicron droplets created near the cloud tops is, indeed, much too broad to match the polarization results of Hansen and Hovenier (1974). The narrow size distribution is more characteristic of condensation growth of the photochemically produced sulfuric acid similar to the model of Hamill *et al.* (1977) for Earth's stratospheric acid haze.

There remain two unsatisfactory features of the photochemical model for the Venus sulfuric acid cloud. First, this model provides no explanation of the cloud droplet number density. In a steady state, the sulfuric acid vapor supersaturation required to produce 1-μm droplets, $\$ \gtrsim 1$ (if $\alpha \sim 10^{-2}$, $\$ \gtrsim 30$), is somewhat lower than in Earth's stratosphere and too low for homogeneous nucleation (cf. Hamill *et al.*, 1977) so that the cloud droplet number density must be controlled by the CCN number density. I show that, even if the CCN are all used, neither meteoritic dust nor surface dust can provide such a large density of CCN, $>10^3$ cm^{-3} at 60 km. The latter source is limited by rapid coagulation near the surface (Rossow, 1977). Second, the source of droplets in this model is near the top of the cloud so that droplet transport to the evaporation level at the bottom by either sedimentation or turbulent diffusion produces a roughly constant cloud mass density with altitude below the source which contradicts the observations from Venera 9 and 10.

In an oxidizing lower atmosphere, if sulfuric acid reforms droplets at the cloud bottom by ordinary condensation like water vapor, then Fig. 6 shows that precipitation sized droplets could form if the cloud bottom is below 50 km and the CCN number density is so small that only <10 cm^{-3} droplets form. The observations of a droplet mean radiu $\ll 10$ μm and a number density $\gg 10$ cm^{-3} throughout this cloud clearly rule out this possibility. Further, the strong chemical reactions among sulfuric acid, sulfur trioxide, and water produce stable embryos which are not simply composed of condensed sulfuric acid (cf. Young, 1973). These strong chemical reactions, together with the involatility of sulfuric acid at these temperatures [for azeotropic sulfuric acid at

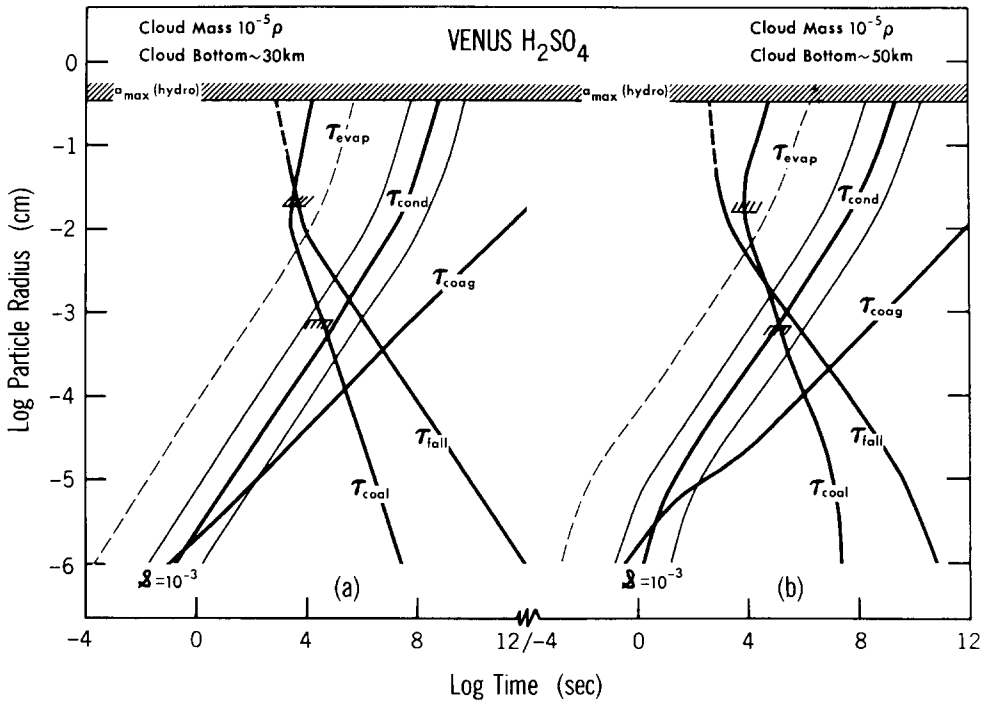

FIG. 6. Same as Fig. 2 for Venus sulfuric acid clouds, with droplets formed at cloud bottom.

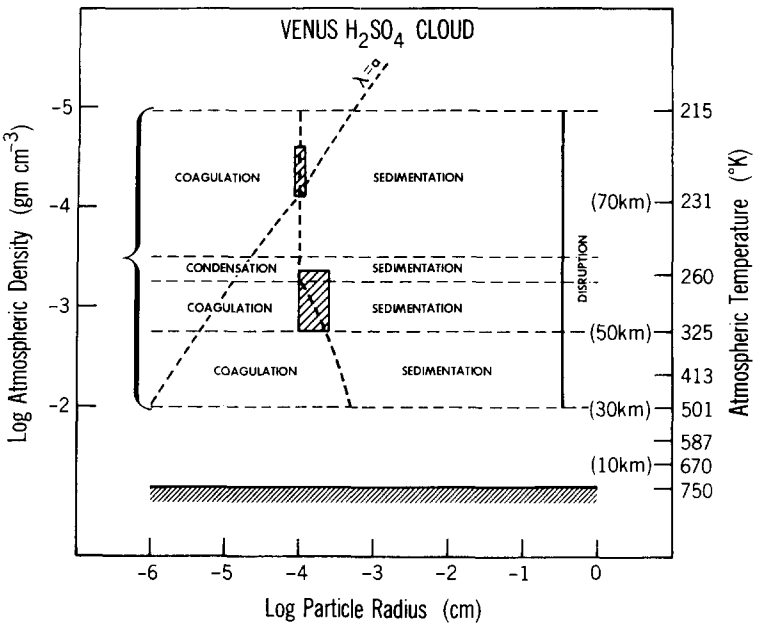

FIG. 7. Same as Fig. 4 for Venus sulfuric acid droplet clouds. Two formation regions are shown, Atmosphere model from Marov (1972).

300 to 500°K, $\rho_s \sim 10^{-2}\rho$ (Young, 1973)], suggest that in Venus' lower atmosphere sulfuric acid droplets are produced by chemical nucleation as they are in Earth's atmosphere, instead of by ordinary nucleation on CCN.

Figures 5 and 6 show that the observed mean droplet radii at 50 and 60 km are consistent with coagulation in a constant mass mixing ratio cloud with growth limited by sedimentation. Further, in a numerical study of this case (Rossow, 1977), I show that the narrow size distribution near the cloud tops is matched by this model when the initial embryos are <0.1 μm in radius. This is much larger than the embryo size in Earth's smogs (e.g., Twomey, 1977; Husar *et al.*, 1972). The most attractive feature of this model is that the observed cloud properties near the top are natural consequences of the total abundance of sulfuric acid, reflected in the cloud mass density, and of the intensity of vertical turbulent mixing in the cloud, characterized by eddy diffusivities $\sim 10^5$–10^6 cm^2 sec^{-1}. The latter, together with coagulation, controls the droplet number density and the former then gives the mean droplet radius (Rossow, 1977).

One unsatisfactory aspect of this model is the disagreement between my results and the nephelometer results of Venera 9 and 10. The former shows a decreasing mean droplet radius and increasing droplet number density with depth which is opposite the Venera results. However, since the nephelometers are insensitive to droplets <0.5 μm in radius, these results are not necessarily contradictory. More observations of the droplet size distribution below 0.5 μm are needed. Although I favor the smog model of the Venus sulfuric acid cloud, the available data are not sufficiently detailed to rule out Prinn's photochemical model as yet. Thus, in Fig. 7 which summarizes this discussion, I show both formation regions.

Throughout the discussion above, I have assumed that the cloud is in a steady state with the consequence that the cloud droplet properties are determined by the balance between growth and removal processes (cf. Fig. 1). If this is correct, the observed variability in the uv albedo near the cloud tops, which occurs on time scales as short as 10^6 sec, cannot be attributed to changes in the droplet properties, except for the possibility that the droplets in the highest parts of the cloud can freeze and melt in <10 sec. The impression that the droplet properties are uniform over the planet and in time supports the steady-state model. However, as is true for Earth's stratospheric haze, this impression may be an average over episodes of growth and decay of the cloud. If the uv variability represents actual cloud droplet formation, the only growth process which is rapid enough is condensation. What the required prolific source of CCN is and what processes control the droplet mean size and number density are questions that would remain unanswered by such a model.

B. The Clouds of Mars

In contrast to the planet-wide, steady-state cloud cover of Venus, the clouds on Mars range from localized, short-lived dust and condensate clouds and fogs to the large, seasonal polar hood clouds and the planet-wide dust storms (Leovy *et al.*, 1973). The atmospheric temperatures and water vapor abundances over the planet (Barker, 1976; Farmer, 1976; Farmer *et al.*, 1976) suggest that most of the condensate clouds are composed of water ice, although this has been confirmed in only one case (Curran *et al.*, 1973). In low and middle latitudes, the water ice clouds are generally small with lifetimes $\sim$1 day (Barth, 1974; Briggs and Leovy, 1974) and usually form as single diffuse patches near the large shield volcanoes in the Tharsis region. This location near some of the highest topographic features suggests that these clouds form in the uplift of the prevailing winds. Curran *et al.* (1973) infer a typical cloud mass density, $\mu \sim 3 \times 10^{-4}\rho = 4.5 \times 10^{-3}$ g m^{-3}, with a mean particle radius, $\bar{a} \sim 2$ μm for these clouds. At high latitudes near the edge of the polar caps, the interaction of strong winds with the topography produces a complex of cloud bands and extensive wave clouds, presumed to be water ice clouds (Briggs and Leovy, 1974). The morphology of all of these clouds suggests an analogy with cirrus clouds on Earth. Low-lying clouds with a cumulus morphology are also observed to form over elevated terrain or at very low temperature, especially in Syria Planum (Briggs and Leovy, 1974; Briggs *et al.*, 1977).

One condensate cloud, twice observed near 25-km altitude, has been identified as a carbon dioxide ice cloud (Herr and Pimentel, 1970). Since carbon dioxide is the major constituent of the Martian atmosphere (Owen and Biemann, 1976), the flow of mass to a growing ice particle does not occur at constant pressure. Instead of a diffusive mass flux of vapor through a background gas, a systematic mass flow occurs greatly complicating the calculation of the mass and heat fluxes. The physics of such a cloud is qualitatively different from any of the clouds studied here. In particular, the expressions for τ_{cond}, (16) and (17), are not valid. Further, the dynamic consequences and feedbacks of even transient carbon dioxide clouds are different because the Clasius–Clapeyron constraint on a saturated vapor cannot simultaneously satisfy the hydrostatic and radiative equilibrium relations. The properties of such clouds are a fascinating new area of cloud physics that requires study, but it is beyond the scope of this paper.

Only the decaying phase of the great dust storm of 1971 has been observed

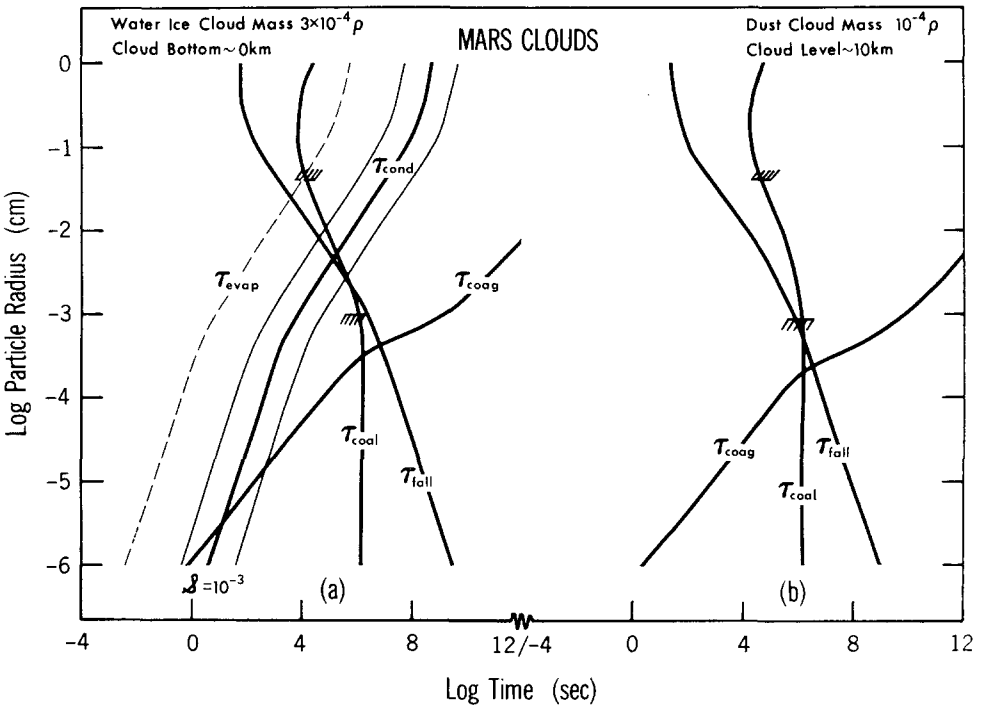

FIG. 8. Same as Fig. 2 for (a) water ice clouds and (b) the decaying phase of the great dust storm on Mars.

from Earth (e.g., Martin, 1974) and from Mariner 9 (Conrath *et al.*, 1973; Conrath, 1974; Gierasch, 1974) in enough detail that some inferences about microphysical processes are possible. The results from the infrared spectrometer on Mariner 9 are consistent with a silicate dust cloud with a mean particle radius, $\bar{a} \sim 2$ μm, and a constant size distribution throughout the decay phase (Toon *et al.*, 9977). The dust mass mixing ratio is $\sim 10^{-4}$ and uniform up to ~50-km altitude (Conrath *et al.*, 1973; Conrath, 1974). The dust cloud cleared in a time $\sim 10^{7}$ sec.

1. Water ice clouds. Figure 8a shows the time constants for a near-surface water ice cloud with $\mu = 3 \times 10^{-4}\rho$. This mass density is similar to the thinnest cirrus clouds on Earth and represents a probable upper limit on the typical water ice cloud mass density on Mars, because most of them occur at somewhat lower atmospheric densities, especially those over elevated regions and because the average water vapor mixing ratio is somewhat smaller though highly variable (Farmer *et al.*, 1977). τ_{cond} is calculated with $\alpha = 1$ and $\mathcal{S} = 10^{-3}$, but the diffuse outline of these clouds suggests that condensation occurs when near-water saturation conditions are attained as in cirrus clouds on Earth. Since Martian atmospheric conditions are generally below the triple point of water, rather strong dynamic cooling is required which may account for the relative scarcity of water clouds and their association with strong winds and wind shears. The higher supersaturations that occur under these conditions, $\mathcal{S} \sim 10^{-1}$, are offset by the small condensation coefficient for water ice at low temperatures, $\alpha \sim 10^{-3}$, which strongly retards condensation in the tenuous atmosphere of Mars (for 2-μm particles at the surface Kn $\sim$ 2). Thus, the $\mathcal{S} = 10^{-4}$

curve for τ_{cond} in Fig. 8a is more appropriate for the growth of ice crystals in these clouds and gives values of $\tau_{cond} \sim 10^4$ sec for 2-μm particles, consistent with observations of cloud formation (Briggs *et al.*, 1977; Pollack *et al.*, 1977).

On two occasions, once at high latitudes in the winter hemisphere and once in an elevated region where atmospheric temperatures are quite low, <200°K, low-lying, cumuliform clouds have been observed (Briggs and Leovy, 1973; Briggs *et al.*, 1977). Briggs and Leovy (1973) suggest that their sharp outline morphology indicates a composition different from the diffuse outline water ice clouds. An alternative explanation is that at these very low temperatures water ice clouds form by direct ice nucleation in a region which is undersaturated with respect to ice on average, but locally saturated by strong, forced convective updrafts. Since the surrounding environment is undersaturated, any ice particles leaving the updraft region immediately evaporate. Similar behavior is observed in small cumulus clouds formed in such convective motions on Earth where the intensity of these motions is great enough to form clouds even under the very low humidity conditions in desserts.

Figure 8a clearly shows that these tenuous clouds cannot form precipitation since $\tau_{fall} < \tau_{coal}$ for particles large enough to overcome the hydrodynamic limit on collisions. (Since Kn $\sim$ 0.5 for 10-μm particles, the interaction of such particles with the atmosphere is only approximately hydrodynamic, but the limit shown is still correct in this regime.) Further, the observed lifetime of these clouds, $\sim 10^5$ sec, is much too short for precipitation to form even if the clouds were ten times more massive. Consequently, total water should remain well mixed in the Martian atmosphere if photochemical and surface chemical reactions are slow compared to dynamic mixing.

Since the water ice clouds form on time scales $\sim 10^4$ sec, much shorter than either their lifetime or the sedimentation time of 2-μm particles (Briggs *et al.*, 1977; Pollack *et al.*, 1977), the growth of the cloud particles cannot be limited by removal processes. (The diffuse outline suggests that small scale turbulent mixing out of the cloud does not limit particle growth.) Thus, the mean particle size of the cloud particles must be controlled by the number density of CCN in the Martian atmosphere. For the values used here, $\bar{a} \sim 2$ μm, $\mu < 3 \times 10^{-4}\rho$, an upper limit on the dust density near the surface is $N < 70$ cm^{-3} which agrees with estimates based on observations by the Viking lander cameras (Pollack *et al.*, 1977). This control of the cloud particle properties by the dust number density, together with the heating of the atmosphere caused by the dust's absorption of sunlight, may explain the complicated interaction between the polar hood clouds and the great dust storm cloud observed by Martin (1975).

Since the higher altitude water ice clouds are relatively scarce and cannot produce precipitation, the influence of the diurnal surface fogs on the distribution of water and other aerosols may be increased (cf. Flasar and Goody, 1976). With fog condensation on the dust particles, the repeated cycle of condensation, sedimentation and evaporation provides an efficient dust removal mechanism. Further, the location of the fogs is strongly temperature dependent, making the dust deposition a local phenomena. As an example, if the fog properties are $\bar{a} \sim 10$ μm and $N \sim 1$ cm^{-3} (Flasar and Goody, 1976), with a lifetime of 10^4 sec and if each ice particle contains a dust particle with $a \sim 0.5$ μm, then 1 cm of dust is deposited by a daily fog in $\sim 3 \times 10^5$ years. These results also suggest that the much larger seasonal deposition of carbon dioxide at

the poles may be one of the dominant processes controlling aerosol distribution, transport, and deposition on Mars.

2. The great dust storm of 1971. Since the decaying dust cloud was at least five scale heights deep and its total optical depth was only <2 (Conrath *et al.*, 1973), the dust properties inferred from the infrared spectrometer observations from Mariner 9 represent vertical averages. Further, since the infrared spectrometer was not sensitive to the submicron part of the size distribution, detected by the ultraviolet spectrometer after nearly complete clearing (Ajello and Pang, 1975), the mean particle radius is only approximate. Figure 8b shows the time constants for a dust cloud at 10 km with $\mu \sim 10^{-4}\rho = 4.5 \times 10^{-4}$ g m^{-3}. The cutoff radius for effective coalescence, shown in the figure, is reasonably accurate since Kn is only ~ 2 for this size particle.

No observations of the microphysical properties of the great dust storm in its growth phase are available so I do not consider this phase here except for its effect on the particle size distribution at the beginning of the decay phase. Theoretical studies (Iversen *et al.*, 1976; Pollack *et al.*, 1976) of the Martian conditions required to raise large quantities of dust find that dust injection is primarily by saltation in very high-speed, fully turbulent winds. Consequently, the dust cloud particle size distribution reflects the particle size distribution in the parent soil up to the size at which the terminal velocity exceeds the turbulent wind velocities. This upper limit on suspended particle radius is ~ 100 μm (Pollack *et al.*, 1976). All observations of airborne aerosols (e.g., Ajello and Pang, 1975; Toon *et al.*, 1977; Pollack *et al.*, 1977) indicate an abundant supply of submicron to micron sized dust on the surface, while the properties of surface soils indicate cohesive particles <100 μm (Shorthill *et al.*, 1976; Moore *et al.*, 1977) and are consistent with a large fraction of even smaller particles (Sagan *et al.*, 1977). Thus the dust cloud particle size distribution should be quite broad, at least near the surface.

Figure 8b shows that effective coalescence of the micron-sized dust particles in the great dust storm cloud is prevented by hydrodynamic forces. Further, the sticking efficiency for micron size and larger particles is essentially zero. If substantial static charges could be created in the cloud (e.g. by ultraviolet radiation), then these two barriers to efficient coalescence could be overcome. The observed mean particle radius and cloud lifetime preclude the consequent rapid growth to radii >10 μm and, consequently, the presence of such static charges in these storms.

The only remaining microphysical process is coagulation for which the sticking efficiency is ≈ 1 even for solid particles. Two observations of the dust cloud decay suggest that coagulation plays an important role in determining the structure of these clouds. First, in Fig. 8 the lifetime of the dust cloud exceeds τ_{fall} for 2-μm particles at all altitudes except near the surface. As discussed in Section IV, Part C, turbulence can only increase the lifetime of cloud particles to the value of τ_{fall} at the bottom of the cloud if the turbulence weakens there. Conrath (1974) shows that just such a model explains the observed clearing of this dust cloud. However, the expected evolution of the particle size distribution caused by the size dependence of the sedimentation rate in the near-surface boundary layer contradicts the second observation, viz., that the particle size distribution remained constant in shape during the clearing (Toon *et al.*, 1977). The near equality of the cloud lifetime, $\sim 10^7$ sec, and τ_{coag} in Fig. 8 suggests that coagulation growth of the submicron dust particles balances the removal of the larger particles by sedimentation and produces a constant size distribution,

in analogy to Earth's tropospheric aerosols at night (Friedlander and Wang, 1966; Husar *et al.*, 1972). This balance also explains why the dust cloud size distribution is narrower than that produced by sedimentation of the soil's broad size distribution. One important consequence of this behavior for modeling the optical properties of this cloud is that the mean particle radius is a very weak function of altitude. This follows from (33) if turbulence maintains a constant particle lifetime $\approx \tau_{coag}$ at all altitudes and a uniform mass mixing ratio such that $N \propto \rho a^{-3}$; then $a \propto \rho^{2/5}$.

3. Summary. Figure 9 summarizes the discussion above. The particle size in the water ice clouds is not limited by sedimentation or particle lifetime but rather by the CCN (or dust) number density. The dust number density and mean radius in the more massive clouds produced in the planet-wide storms are controlled by turbulence and coagulation. The large hatched region in Fig. 9 reflects the uncertainties about the dust size distribution.

C. The Clouds of Jupiter

Even though the recent Pioneer 10 and 11 missions have greatly increased the total knowledge of Jupiter's atmosphere [see especially the reviews in *Jupiter* (T. Gehrels, Ed.)], knowledge of the complex cloud system is almost completely lacking. The only solid facts are that there is a very tenuous, ultraviolet-absorbing haze layer composed of submicron ($a < 0.1$ μm) particles in the stratosphere (e.g. Smith *et al.*, 1977) and that the blue–white clouds are ammonia ice clouds (Anderson and Pipes, 1971; Ohring, 1973). The only attempt to deduce the mean particle size of the ammonia ice clouds (Morozhenko and Yanovitskii, 1973) is very model dependent (Coffeen and Hansen, 1974) and contains unknown contributions from the stratospheric haze. Thus the discussion of Jupiter's clouds is not constrained by observations.

Simple equilibrium chemistry models of Jupiter's atmosphere with solar abundances predict many condensate cloud layers (e.g., Weidenschilling and Lewis, 1973; Sagan and Salpeter, 1976; Prinn and Owen, 1976), while photochemical models predict the existence of several more haze forming substances in the stratosphere (e.g., Strobel, 1975). I discuss the detected ammonia ice clouds near 140°K temperature level and the pre-

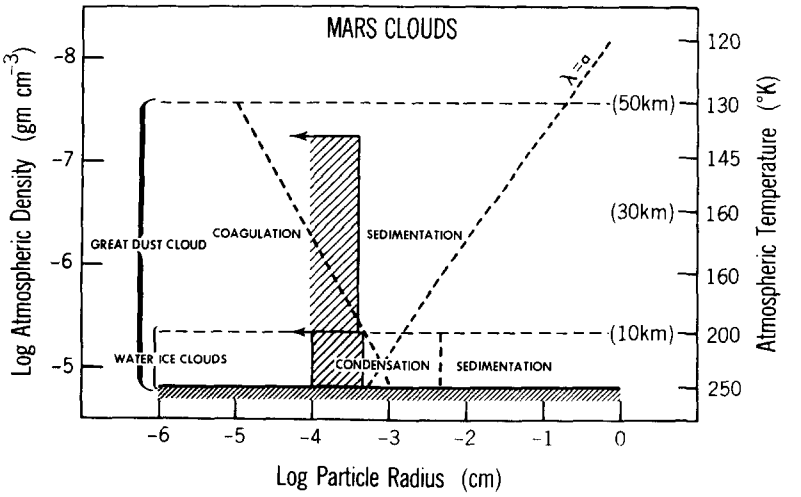

FIG. 9. Same as Fig. 4 for Mars clouds. Atmosphere model from Eshleman (1970).

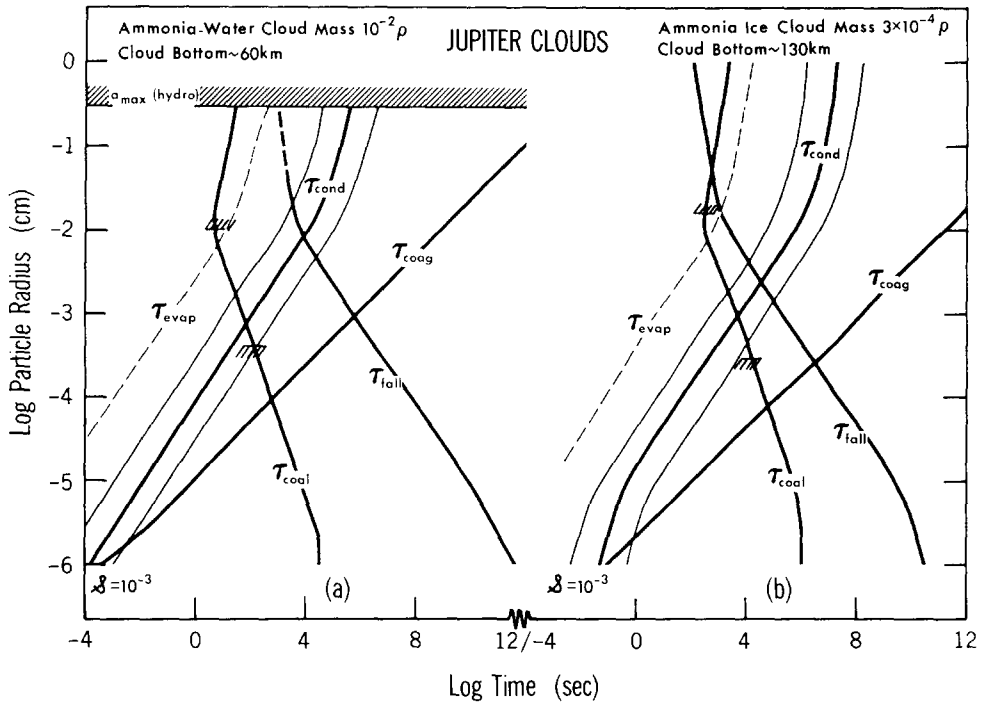

FIG. 10. Same as Fig. 2 for (a) liquid ammonia–water clouds and (b) ammonia ice clouds on Jupiter.

dicted ammonia–water solution cloud near the 280°K level, potentially the most massive of the condensate clouds in the upper atmosphere (Weidenschilling and Lewis, 1973).

1. Ammonia–water clouds. Figure 10a displays the time constants at the bottom of a solar abundance ammonia–water solution cloud which is a liquid in its lowest layers. The chemical behavior of the ammonia–water system is much simpler than that of the sulfuric acid–water system because the interaction between these two substances is much weaker. This is demonstrated by the fact that the presence of ammonia (in this case the abundance of ammonia is 10% that of water) does not change the saturation vapor pressure for water condensation by more than an order of magnitude (Stauffer and Kiang, 1974), in contrast to the sulfuric acid–water system. Further, since ammonia and water vapor are present in roughly comparable amounts over solutions, the composition of the condensed phase is most strongly controlled by the temperature and the relative abundance of ammonia and water, rather than by the temperature and the absolute abundance of one substance. These two vapors behave rather like a single condensing vapor with a more complex temperature dependence of ρ_s. The natural analogy for these clouds, then, is the tropospheric water clouds on Earth.

It is hard to avoid the conclusion that these very dense clouds, $\mu = 10^{-2}\rho \approx 10$ g m^{-3}, produce precipitation. Even if the CCN number density were so large that only 1-μm droplets are produced initially, the difference in the equilibrium vapor density between different size droplets caused by $\mathcal{S}_{curv}$ in (8) can amount to $\mathcal{S} \sim 10^{-4}$ and can produce rapid growth of the larger droplets at the expense of

the smaller droplets. By this vapor exchange, the droplet number density is reduced and the mean droplet radius increased. Furthermore, since the upper portions of these clouds are composed of ice (Weidenschilling and Lewis, 1973), the Bergeron process strongly encourages precipitation formation. Finally, the hydrodynamic limiting radius for coalescence is a factor of two smaller than on Earth primarily because of Jupiter's stronger gravity and smaller atmospheric viscosity. All of these factors lead to rapid formation of precipitation on a time scale $<10^3$ sec.

Figure 10a shows that $\tau_{coal} \ll \tau_{fall}$ so that the precipitation size distribution is limited by disruptive collisions at a mean radius ~ 100 μm. However, if the rainfall rate is large, the droplet size distribution is very broad and the mean radius exceeds this limit (cf. Marshall and Palmer, 1948). Since these large raindrops (100 μm $< a <$ 4000 μm) fall at least half a scale height before evaporating (cf. Fig. 10a), ammonia, water, all soluble gases, and all other aerosols throughout at least one scale height in Jupiter's atmosphere are rapidly transported downward on a time scale certainly $<10^4$ sec. Consequently, the mixing ratios of all these substances must decrease with altitude above the precipitation evaporation level even in the presence of strong vertical mixing. (A vertical eddy diffusivity $>10^9$ cm^2 sec^{-1} is required to oppose the downward transport by precipitation.) In particular, the total mass densities of ammonia and water are constrained to follow closely their saturation vapor density profiles. Since large scale updrafts are so efficiently stripped of these two substances, dry downdrafts and cloud free regions result.

The rapid redistribution of heat energy by latent heat release in the cloud and latent heat absorption in the precipitation evaporation region, together with the density changes involved in condensing and evaporating almost 1% of the atmosphere's mass, has very important consequences for the large scale dynamics of Jupiter's atmosphere (Gierasch, 1976) and for the structure of the ammonia–water clouds themselves. If the redistribution of heat is such that a stable temperature lapse rate is produced and small-scale convective motions are suppressed, then the clouds would resemble precipitating stratus clouds with vapor supplied only by very gentle turbulence or by the vertical motions associated with large-scale circulations. The rainfall rate would be low and the dynamic influence of this quiet system would be confined to less than one scale height in the atmosphere. On the other hand, if the latent heating in the cloud is such that small-scale convective overturning is strongly enhanced, then the clouds would resemble massive, precipitating cumulus clouds, or thunderstorms, will all of the associated phenomena, viz., violent turbulent motions, very high rainfall rates, hail production, and strong electrical discharges. The influence of this type of cloud system would extend over several scale heights in the atmosphere.

2. Ammonia ice clouds. The time constants in Fig. 10b are for an ammonia ice cloud with $\mu = 3 \times 10^{-4}\rho = 6 \times 10^{-2}$ g m^{-3}, approximately equal to the saturation vapor density of ammonia at 140°K. This vapor density is consistent with the ammonia abundance deduced from infrared emission spectra (Ohring, 1973) and with the chemical equilibrium model of Weidenschilling and Lewis (1973), but the actual abundance and distribution may be very different since ammonia is destroyed photochemically in the upper atmosphere (Prinn and Owen, 1976).

The mass density of these ice clouds suggests an analogy with dense, precipitating cirrus clouds on Earth. The fact that the clouds form at temperatures only some tens of degrees lower than the freezing temperature of ammonia (although the cloud

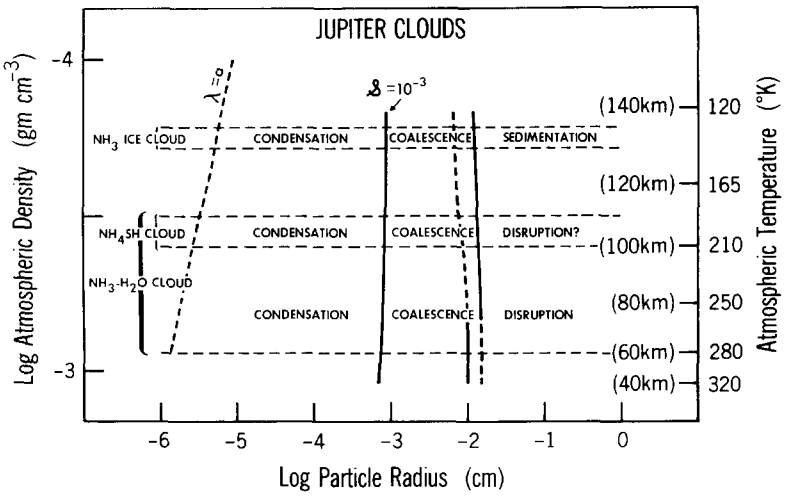

FIG. 11. Same as Fig. 4 for Jupiter clouds. Double line between coalescence and disruption regimes indicates uncertainty of particle phase. Atmosphere model from Weidenschilling and Lewis (1973).

location is not that well known) means that, like water ice, these ice particles are nucleated as supercooled liquid droplets with $s \gg 10^{-3}$ for subsequent growth. The larger supersaturation would more than compensate for a low condensation coefficient ($\alpha > 10^{-3}$ has little effect on the growth rate of particles >10 μm in radius) or for a large CCN number density. Although these uncertainties cannot be removed at present, it is probable that these clouds produce ammonia snow on a time scale $\sim 10^4$ sec as Fig. 10b shows. Since large ice particle terminal velocities are generally lower than those of spheres, the disruptive collision limit to coalescence growth in Fig. 10b is too low. Thus, in contrast to the lower ammonia–water clouds, coalescence growth is limited by sedimentation in these clouds. The consequent stripping of ammonia from updrafts by precipitation is consistent with the existence of cloud-free regions on Jupiter. If only micron size particles were present in the cloud, then even weak dynamic mixing on a time scale $\sim 10^7$ sec could maintain a uniform ammonia mixing ratio.

3. Summary and comments. The cloud mass densities predicted by chemical equilibrium models for Jupiter's atmosphere depend on the assumed atmospheric composition and temperature-pressure structure, but all of these models show three condensate clouds of roughly comparable mass density above the 10-bar pressure level. The coalescence time constant scales with the inverse of the mass density, so Fig. 10 suggests that the ammonium hydrosulfide cloud, between the ammonia ice and ammonia–water clouds, also produces precipitation on a time scale $\sim 10^4$ sec. Further, since these clouds are only a scale height apart in altitude and composed of chemically reactive substances, the precipitation from one cloud can stimulate precipitation in a lower cloud. This is likely to be an extremely difficult cloud system to understand. Figure 11 summarizes these results. The expected mean particle radius in all of these clouds is >10 μm with coalescence growth producing precipitation.

VIII. SUMMARY

1. Tropospheric water clouds on Earth are the prototype cooling clouds. Because of the relatively high saturation vapor

density of water, nucleation of the liquid phase occurs efficiently by heterogeneous processes at very low supersaturations. Nucleation of the ice phase is much less efficient with the result that it generally occurs as the nucleation of supercooled droplets which freeze. In a "dirty" atmosphere, $S \sim 10^{-3\pm1}$ is probably typical for condensation with the cloud particle number density controlled by the number density of CCN.

2. Precipitation is formed only by coalescence. For liquid water clouds, the critical mass density for precipitation is a consequence of the Stokes number size limit on efficient coalescence. For water ice clouds, coalescence is limited by sedimentation.

3. The sulfuric acid hazes in the troposphere and stratosphere of Earth are prototype chemical clouds. The nucleation processes for involatile substances are not well understood since even heterogeneous nucleation requires extremely high supersaturations. The primary growth process is condensation if heterogeneous nucleation occurs and coagulation if some other process occurs. The evolution of such tenuous hazes in the absence of particle production is always by coagulation. This important class of clouds needs much more study.

4. Dust storms on Earth are the prototype dust clouds but their microphysical processes have not been studied.

5. The sulfuric acid cloud on Venus is a chemical cloud like the sulfuric acid hazes on Earth. The cloud droplets and the cloud mass density are too small for coalescence to play any role in the clouds. Brownian coagulation, with a time constant $\sim 10^7$ sec, predominates away from the droplet formation region. The two models of the chemistry of sulfuric acid lead to two models of the droplet formation: photochemical production of vapor with condensation growth of the droplets near the cloud top (cf. the stratospheric sulfuric acid haze) and a chemically "stable" vapor with coagulation of the hydrated sulfuric acid particles near the cloud bottom (cf. the tropospheric sulfuric acid haze). Recent observations of the vertical cloud structure favor the latter model.

6. The water ice clouds on Mars are tenuous, nonprecipitating cirrus clouds like those in Earth's upper troposphere. Their mean particle radius and particle number density are controlled by the number density of surface dust particles which act as CCN. Surface fogs may control the dust number density in the atmosphere as well as the location of dust deposition.

7. The decaying phase of the great dust storm of 1971 resembles the nighttime evolution of aerosols on Earth with sedimentation at the surface from a turbulent cloud and coagulation that maintains a constant particle size distribution. The coagulation time constant is $\sim 3 \times 10^6$ sec.

8. All of the condensate clouds in Jupiter's upper atmosphere, predicted by chemical equilibrium models, are cooling clouds that resemble massive liquid water and water ice clouds on Earth. They produce precipitation on time scales $\lesssim 10^4$ sec. The dynamics of this region of the atmosphere is probably quite complex, involving possible cumulus dynamics, strong vertical transports of aerosols and heat by the precipitation, and interaction between the cloud layers.

ACKNOWLEDGMENTS

I wish to thank Peter J. Gierasch and Gareth P. Williams for their support and encouragement through the long writing of this paper. I also wish to thank Frank B. Lipps, Kikuro Miyakoda, and an anonymous reviewer for many helpful comments and suggestions and to thank Lynne M. Kemen for her help in editing and proofing the manuscript. Thanks are also due to Carolyn Longmuir for her patient typing of many versions of this paper and to Philip G. Tunison and John N. Conner for the graphics. This work was supported in part by NASA Grant NGL-33-010-186 and NOAA Grant 04-3-022-33.

REFERENCES

ABBOTT, C. E. (1974). Experimental cloud droplet collection efficiencies. *J. Geophys. Res.* **79**, 3098–3100.

*ABBOTT, C. E. (1977). A survey of waterdrop interaction experiments. *Rev. Geophys. Space Phys.* **15**, 363–374.

ABRAHAM, F. F. (1968). A reexamination of homogeneous nucleation theory: Thermodynamic aspects. *J. Atmos. Sci.* **25**, 47–53.

ABRAHAM, F. F. (1970). Functional dependence of drag coefficient of a sphere on Reynolds number. *Phys. Fluids.* **13**, 2194–2195.

AJELLO, J. M., AND PANG, K. D. (1975). Mariner 9 ultraviolet spectrometer experiment: Scattering properties of Hellas. *Icarus* **26**, 332–340.

ALLEN, L. B., AND KASSNER, J. L. (1969). The nucleation of water vapor in the absence of particulate matter and ions. *J. Colloid Interface Sci.* **30**, 81–93.

ALMEDIA, F. C. DE (1977). Collision efficiency, collision angle and impact velocity of hydrodynamically interacting cloud drops: A numerical study. *J. Atmos. Sci.* **34**, 1286–1292.

ANDERSON, R. C., AND PIPES, J. G. (1971). Jovian ultraviolet reflectivity compared to absorption by solid ammonia. *J. Atmos. Sci.* **28**, 1086–1087.

*BAGNOLD, R. A. (1941). *The Physics of Blown Sand and Desert Dunes.* Methuen, London.

BARKER, E. S. (1976). Martian atmospheric water vapor observations: 1972–74 apparition. *Icarus* **28**, 247–268.

BARTH, C. A. (1974). Atmosphere of Mars. *Ann. Rev. Earth Planet. Sci.* **2**, 333–367.

BAYEWITZ, M. H., YERUSHALMI, J., KATZ, S., AND SHINNAR, R. (1974). The extent of correlations in a stochastic coalescence process. *J. Atmos. Sci.* **31**, 1604–1614.

*BEARD, K. V. (1976). Terminal velocity and shape of cloud and precipitation drops. *J. Atmos. Sci.* **33**, 851–864.

BEARD, K. V., AND PRUPPACHER, H. R. (1971). A wind tunnel investigation of collection kernels for small water drops in air. *Quart. J. Roy. Meteorol. Soc.* **97**, 242–248.

BERRY, E. X (1967). Cloud droplet growth by collection. *J. Atmos. Sci.* **24**, 688–701.

BERRY, E. X, AND PRANGER, M. R. (1974). Equations for calculating terminal velocities of water drops. *J. Appl. Meteorol.* **13**, 108–113.

BERRY, E. X, AND REINHARDT, R. L. (1974). An analysis of cloud drop growth by collection: Part IV. A new parameterization. *J. Atmos. Sci.* **31**, 2127–2135.

BRAHAM, R. R. (1976). CCN Spectra in C–k space. *J. Atmos. Sci.* **33**, 343–345.

BRAZIER-SMITH, P. R., JENNINGS, S. G., AND LATHAM, J. (1972). The interaction of falling water drops: Coalescence. *Proc. Roy. Soc. London Ser. A* **326**, 393–408.

BRIGGS, G., KLAASEN, K., THORPE, T., WELLMAN, J., AND BAUM, W. (1977). Martian dynamical phenomena during June–November 1976: Viking orbiter imaging results. *J. Geophys. Res.* **82**, 4121–4149.

BRIGGS, G., AND LEOVY, C. B. (1974). Mariner 9 observations of the Mars north polar hood. *Bull. Amer. Meteorol. Soc.* **55**, 278–296.

BROCK, J. R. (1966). Diffusion to particles in the near free molecule region. *J. Colloid Interface Sci.* **22**, 513–516.

BROCK, J. R. (1972). Condensational growth of atmospheric aerosols. *J. Colloid Interface Sci.* **39**, 32–36.

CADLE, R. D., AND GRAMS, G. W. (1975). Stratospheric aerosol particles and their optical properties. *Rev. Geophys. Space Phys.* **13**, 475–501.

CAPORALONI, M., TAMPIERI, F., TROMBELLI, F., AND VITTORI, O. (1975). Transfer of particles in nonisotropic air turbulence. *J. Atmos. Sci.* **32**, 565–568.

CARSTENS, J. C., PODZIMEK, J., AND SAAD, A. (1974). On the analysis of the condensation growth of a stationary cloud droplet in the vicinity of activation. *J. Atmos. Sci.* **31**, 592–596.

*CASTLEMAN, A. W. (1974). Nucleation processes and aerosol chemistry. *Space Sci. Rev.* **15**, 547–589.

CHAMBERLAIN, A. C. (1975). The movement of particles in plant communities. In *Vegetation and the Atmosphere* (J. L. Monteith, Ed.), pp. 155–203. Academic Press, New York.

CHANDRASEKHAR, S. (1943). Stochastic problems in physics and astronomy. *Rev. Mod. Phys.* **15**, 1–90.

*CHEPIL, W. S., AND WOODRUFF, N. P. (1963). The physics of wind erosion and its control. *Advan. Agron.* **15**, 211–302.

CHOULARTON, T. W., AND LATHAM, J. (1977). Measurements of the deposition coefficient for ice, and its application to cirrus seeding. *Quart. J. Roy. Meteorol. Soc.* **103**, 307–318.

COFFEEN, D. L., AND HANSEN, J. E. (1974). Polarization studies of planetary atmospheres. In *Planets, Stars and Nebulae Studied with Photopolarimetry* (T. Gehrels, Ed.), pp. 518–581. U. of Arizona Press, Tucson.

CONRATH, B. J. (1974). Thermal structure of the Martian atmosphere during the dissipation of the dust storm of 1971. *Icarus* **24**, 36–46.

CONRATH, B. J., CURRAN, R., HANEL, R., KUNDE, V., MAGUIRE, W., PEARL, J., PIRRAGLIA, J., WELKER, J., AND BURKE, T. (1973). Atmospheric and surface properties of Mars obtained by infrared spectroscopy on Mariner 9. *J. Geophys. Res.* **78**, 4267–4278.

CORN, M. (1966). Adhesion of particles. In *Aerosol Science* (C. N. Davies, Ed.), pp. 359–392. Academic Press, New York.

CURRAN, R. J., CONRATH, B. J., HANEL, R. A., KUNDE, V. G., AND PEARL, J. C. (1973). Mars: Mariner 9 spectroscopic evidence for H_2O ice clouds. *Science* **182**, 381–383.

DAEE, M., LUND, L. H., PLUMMER, P. L. M., KASSNER, J. L., AND HALE, B. N. (1972). Theory of nucleation of water. I. Properties of some clathrate-like cluster structures. In *Aerosols and Atmospheric Chemistry* (G. M. Hidy, Ed.), pp. 91–104. Academic Press, New York.

DAHNEKE, B. (1973). Comments on "Collisions of small cloud droplets: Gas kinetics effects." *J. Atmos. Sci.* **30**, 506–507.

DAVIES, C. N. (1966). Deposition from moving aerosols. In *Aerosols Science* (C. N. Davies, Ed.), pp. 393–446. Academic Press, New York.

DAVIS, M. H. (1972). Collisions of small cloud droplets: Gas kinetic effects. *J. Atmos. Sci.*, **29**, 911–915.

DAVIS, M. H., AND SARTOR, J. D. (1967). Theoretical collision efficiencies for small cloud droplets in Stokes flow. *Nature* **215**, 1371–1372.

DUFOUR, L., AND DEFAY, R. (1963). *Thermodynamics of Clouds*. Academic Press, New York.

ESHLEMAN, V. R. (1970). Atmospheres of Mars and Venus: A review of Mariner 4 and 5 and Venera 4 experiments. *Radio Sci.* **5**, 325–332.

FARMER, C. B. (1976). Liquid water on Mars. *Icarus* **28**, 279–289.

FARMER, C. B., DAVIES, D. W., HOLLAND, A. L., LAPORTE, D. D., AND DOMS, P. E. (1977). Mars: Water vapor observations from the Viking orbiters. *J. Geophys. Res.* **82**, 4225–4248.

FITZGERALD, J. W. (1972). A study of the initial phase of cloud droplet growth by condensation and comparison between theory and observation. Ph.D. thesis, University of Chicago.

FITZGERALD, J. W. (1973). Dependence of the supersaturation spectrum of CCN on aerosol size distribution and composition. *J. Atmos. Sci.* **30**, 628–634.

FLASAR, F. M., AND GOODY, R. M. (1976). Diurnal behavior of water on Mars. *Planet. Space Sci.* **24**, 161–181.

FLETCHER, N. H. (1962). *The Physics of Rainclouds*. Cambridge Univ. Press, Cambridge.

FOOTE, G. B. (1975). The water-drop rebound problem: Dynamics of collision. *J. Atmos. Sci.* **32**, 390–402.

FRENKEL, J. (1946). *Kinetic Theory of Liquids*. Clarendon Press, Oxford.

FRIEDLANDER, S. K., AND WANG, C. S. (1966). The self-preserving particle size distribution for coagulation by Brownian motion. *J. Colloid Interface Sci.* **22**, 126–132.

FRIEND, J. P., LEIFER, R., AND TRICHNON, M. (1973). On the formation of stratospheric aerosols. *J. Atmos. Sci.* **30**, 465–479.

*FUCHS, N. A. (1959). *Evaporation and Droplet Growth in Gaseous Media* (R. S. Bradley, Ed.; J. M. Pratt, Transl.). Pergamon, New York.

*FUCHS, N. A. (1964). *The Mechanics of Aerosols* (C. N. Davies, Ed.; R. E. Daisley and M. Fuchs, Trans.). Pergamon, Oxford.

FUCHS, N. A., AND SUTUGIN, A. G. (1970). *Highly Dispersed Aerosols*. Ann Arbor Science Pub., Ann Arbor, Mich.

FUKUTA, N., AND WALTER, L. A. (1970). Kinetics of hydrometeor growth from a vapor-spherical model. *J. Atmos. Sci.* **27**, 1160–1172.

GEHRELS, T. (Ed.) (1976). *Jupiter*. Univ. of Arizona Press, Tuscon.

GERBER, H. E. (1976). Relationship of size and activity for AgI smoke particles. *J. Atmos. Sci.* **33**, 667–677.

GIERASCH, P. J. (1974). Martian dust storms. *Rev. Geophys. Space Phys.* **12**, 730–734.

GIERASCH, P. J. (1976). Jovian meteorology: Large-scale moist convection. *Icarus* **29**, 445–454.

GILLESPIE, D. T. (1975). Three models for the coalescence growth of cloud drops. *J. Atmos. Sci.* **32**, 600–607.

GILLETTE, D. A., BLIFFORD, I. H., AND FRYREAR, D. W. (1974). The influence of wind velocity on the size distributions of aerosols generated by wind erosion of soils. *J. Geophys. Res.* **79**, 4068–4075.

GUNN, R. (1965). Collision characteristics of freely falling water drops. *Science* **150**, 695–701.

HAMILL, P., TOON, O. B., AND KIANG, C. S. (1977). Microphysical processes affecting stratospheric aerosol particles. *J. Atmos. Sci.* **34**, 1104–1119.

HANSEN, J. E., AND HOVENIER, J. W. (1974). Interpretation of the polarization of Venus. *J. Atmos. Sci.* **31**, 1137–1160.

HAPKE, B. (1976). Photometry of Venus from Mariner 10. *J. Atmos. Sci.* **33**, 1803–1915.

HERR, K. C., AND PIMENTEL, G. C. (1970). Evidence for solid carbon dioxide in the upper atmosphere of Mars. *Science* **167**, 47–49.

HIDY, G. M. (1965). On the theory of the coagulation of noninteracting particles in Brownian motion. *J. Colloid Sci.* **20**, 123–144.

HIDY, G. M., AND BROCK, J. R. (1965a). Some remarks about the coagulation of aerosol particles by Brownian motion. *J. Colloid Interface Sci.* **20**, 477–491.

HIDY, G. M., AND BROCK, J. R. (1965b). Collision-rate theory and the coagulation of free-molecule aerosols. *J. Appl. Phys.* **36**, 1857–1862.

HO, W., HIDY, G. M., AND GOVAN, R. M. (1974). Microwave measurements of the liquid water

content of atmospheric aerosols. *J. Appl. Meteor.* **13**, 871–879.

*Hobbs, P. V. (1974). *Ice Physics.* Clarendon Press, Oxford.

Husar, R. B., Whitby, K. T., and Liu, B. Y. H. (1972). Physical mechanisms governing the dynamics of Los Angeles smog aerosol. In *Aerosols and Atmospheric Chemistry* (G. M. Hidy, Ed.), pp. 271–284. Academic Press, New York.

Iversen, J. D., Pollack, J. B., Greeley, R., and White, B. R. (1976). Saltation threshold on Mars: The effect of interparticle forces, surface roughness, and low atmospheric density. *Icarus*, **29**, 381–393.

Jayaratne, O. W., and Mason, B. J. (1964). The coalescence and bouncing of water drops at an air/water interface. *Proc. Roy. Soc. London Ser. A* **280**, 545–565.

Jiusto, J. E., and Weickmann, H. K. (1973). Types of snowfall. *Bull. Amer. Meteorol. Soc.* **54**, 1148–1162.

Jonas, P. R., and Goldsmith, P. (1972). The collection efficiencies of small droplets falling through a sheared air flow. *J. Fluid Mech.* **52**, 593–608.

Jonas, P. R., and Mason, B. J. (1974). The evolution of droplet spectra by condensation and coalescence in cumulus clouds. *Quart. J. Roy. Meteorol. Soc.* **100**, 286–295.

Junge, C. E. (1963). *Air Chemistry and Radioactivity.* Academic Press, New York.

Junge, C. E., and McLaren, E. (1971). Relationship of cloud nuclei spectra to aerosol size distribution and composition. *J. Atmos. Sci.* **28**, 382–390.

Keldysh, M. V. (1977). Venus exploration with the Venera 9 and Venera 10 spacecraft. *Icarus* **30**, 605–625.

Klett, J. D., and Davis, M. H. (1973). Theoretical collision efficiencies of cloud droplets at small Reynolds numbers. *J. Atmos. Sci.* **30**, 107–117.

Lacis, A. A. (1975). Cloud structure and heating rates in the atmosphere of Venus. *J. Atmos. Sci.* **32**, 1107–1124.

Latham, J., and Reed, R. L. (1977). Laboratory studies of the effects of mixing on the evolution of cloud droplet spectra. *Quart. J. Roy. Meteorol. Soc.* **103**, 297–306.

Leovy, C. B., Briggs, G. A., and Smith, B. A. (1973). Mars atmosphere during the Mariner 9 extended mission: Television results. *J. Geophys. Res.* **78**, 4252–4266.

Levin, Z., Neiburger, M., and Rodriguez, L. (1973). Experimental evaluation of collection and coalescence efficiencies of cloud drops. *J. Atmos. Sci.* **30**, 944–946.

Lin, C. L., and Lee, S. C. (1975). Collision efficiency of water drops in the atmosphere. *J. Atmos. Sci.* **32**, 1412–1418.

Liu, B. Y. H., and Whitby, K. T. (1968). Dynamic equilibrium in self-preserving aerosols. *J. Colloid Interface Sci.* **26**, 161–165.

Marov, M. Ya. (1972). Venus: A perspective at the beginning of planetary exploration. *Icarus* **16**, 415–461.

Marov, M. Ya., Avduevsky, N. S., Borodin, N. F., Ekonomov, A. P., Kerzhanovich, V. V., Lysov, V. P., Moshkin, B. Ye., Rozhdestvensky, M. K., and Ryabov, O. L. (1973). Preliminary results on the Venus atmosphere from the Venera 8 descent module. *Icarus* **20**, 407–421.

Marshall, J. S., and Palmer, W. McK. (1948). The distribution of raindrops with size. *J. Meteorol.* **5**, 165–166.

Martin, L. J. (1974). The major Martian yellow storm of 1971. *Icarus* **22**, 175–188.

Martin, L. J. (1975). North polar hood observations during Martian dust storms. *Icarus* **26**, 341–352.

Martonchik, J. V., and Beer, R. (1975). Analysis of spectrophotometric observations of Venus in the 3–4 micron region. *J. Atmos. Sci.* **32**, 1151–1156.

*Mason, B. J. (1971). *The Physics of Clouds.* Clarendon Press, Oxford.

McTaggart-Cowan, J. D., and List, R. (1975). Collision and breakup of water drops at terminal velocity. *J. Atmos. Sci.* **32**, 1401–1411.

Meek, C. C., and Jones, B. G. (1973). Studies of the behavior of heavy particles in a turbulent fluid flow. *J. Atmos. Sci.* **30**, 239–244.

Moore, H. J., Hutton, R. E., Scott, R. F., Spitzer, C. R., and Shorthill, R. W. (1977). Surface materials of the Viking landing sites. *J. Geophys. Res.* **82**, 4497–4523.

Morozhenko, A. V., and Yanovitskii, E. G. (1973). The optical properties of Venus and the Jovian planets I. The atmosphere of Jupiter according to polarimetric observations. *Icarus* **18**, 583–592.

Nielsen, A. E. (1964). *Kinetics of Nucleation.* Pergamon, New York.

Ohring, G. (1973). The temperature and ammonia profiles in the Jovian atmosphere from inversion of the Jovian emission spectrum. *Astrophys. J.* **184**, 1027–1040.

O'Leary, B. (1975). Venus: Vertical structure of stratospheric hazes from Mariner 10 pictures. *J. Atmos. Sci.* **32**, 1091–1100.

Owen, T., and Biemann, K. (1976). Composition of the atmosphere at the surface of Mars: Detection of Argon-36 and preliminary analysis. *Science*, **193**, 801–803.

PASQUILL, F. (1974). *Atmospheric Diffusion*, pp. 252–269. Ellis Horwood Ltd., Chichester.

PICH, J., FRIEDLANDER, S. K., AND LAI, F. S. (1970). The self-preserving size distribution for coagulation by Brownion motion III. Smoluchowski coagulation and simultaneous Maxwellian condensation. *Aerosol Sci.* **1**, 115–126.

PODZIMEK, J., AND SAAD, A. N. (1975). Retardation of condensation nuclei growth by surfactant. *J. Geophy. Res.* **80**, 3386–3392.

POLLACK, J. B., COLLOURN, D., KAHN, R., HUNTER, J., CAMP, W. V., CARLSTON, C. E., AND WOLF, M. R. (1977). Properties of aerosols in the Martian atmosphere, as inferred from Viking lander imaging data. *J. Geophys. Res.* **82**, 4479–4496.

POLLACK, J. B., STRECKER, D. W., WITTEBORN, F. C., ERICKSON, E. F., AND BALDWIN, B. J. (1978). Properties of the clouds of Venus, as inferred from airborne observations of its near infrared reflectivity spectrum. *Icarus*, **34** 28–45.

POLLACK, J. R., HABERLE, R., GREELEY, R., AND IVERSEN, J. (1976). Estimates of the windspeeds required for particles motion on Mars. *Icarus* **29**, 395–417.

PRANDTL, L. (1953). *Essentials of Fluid Dynamics*. Blackie, London.

PRINN, R. G. (1973). Venus: Composition and structure of the visible clouds. *Science* **182**, 1132–1135.

PRINN, R. G., AND OWEN, T. (1976). Chemistry and spectroscopy of the Jovian atmosphere. In *Jupiter* (T. Gehrels, Ed.), pp. 319–371. Univ. of Arizona Press, Tuscon.

PRUPPACHER, H. R., AND PITTER, R. L. (1971). A semi-empirical determination of the shape of cloud and rain drops. *J. Atmos. Sci.* **28**, 86–94.

ROOTH, C. (1960). A statistical study of cloud droplet growth by condensation. In *Physics of Precipitation* (H. Weickmann, Ed.), pp. 220–225. Geophys. Monograph No. 5, Amer. Geophys. Union.

ROSSOW, W. B. (1977). The clouds of Venus: II. An investigation of the influence of coagulation on the observed droplet size distribution. *J. Atmos. Sci.* **34**, 417–431.

ROSSOW, W. B., AND SAGAN, C. (1975). Microwave boundary conditions on the atmosphere and clouds of Venus. *J. Atmos. Sci.* **32**, 1164–1176.

SAAD, A. N., PODZIMEK, J., AND CARSTENS, J. C. (1976). Some remarks on modeling of the early stage of cloud formation in a simulation chamber. *J. Appl. Meteorol.* **15**, 145–156.

SAFFMAN, P. G., AND TURNER, J. S. (1956). On the collision of drops in turbulent clouds. *J. Fluid Mech.* **1**, 16–30.

SAGAN, C., AND BAGNOLD, R. A. (1975). Fluid transport on Earth and aeolian transport on Mars. *Icarus* **26**, 209–218.

SAGAN, C., PIERI, D., FOX, P., ARVIDSON, R. E., AND GUINNESS, E. A. (1977). Particle motion on Mars inferred from the Viking lander cameras. *J. Geophys. Res.* **82**, 4430–4438.

SAGAN, C., AND SALPETER, E. E. (1976). Particles, environments and possible ecologies in the Jovian atmosphere. *Astrophys. J. Suppl.* **32**, 737–755.

SARTOR, J. D., AND ABBOTT, C. E. (1975). Prediction and measurement of the accelerated motion of water drops in air. *J. Appl. Meteorol.* **14**, 232–239.

SCHLAMP, R. J., GROVER, S. N., PRUPPACHER, H. R., AND HAMIELEC, A. E. (1976). A numerical investigation of the effect of electric charges and vertical external electric fields on the collision efficiency of cloud drops. *J. Atmos. Sci.* **33**, 1747–1755.

SCHLAMP, R. J., PRUPPACHER, H. R., AND HAMIELEC, A. E. (1975). A numerical investigation of the efficiency with which simple columnar ice crystals collide with supercooled water drops, *J. Atmos. Sci.* **32**, 2330–2337.

SCOTT, W. D., AND LEVIN, Z. (1975). A comparison of formulations of stochastic collection. *J. Atmos. Sci.* **32**, 843–847.

SCOTT, W. T. (1967). Poisson statistics in distributions of coalescing droplets. *J. Atmos. Sci.* **24**, 221–225.

SCOTT, W. T. (1968). Analytic studies of cloud droplet coalescence I. *J. Atmos. Sci.* **25**, 54–65.

*SEDUNOV, YU. S. (1974). *Physics of Drop Formation in the Atmosphere.* (P. Greenberg, Ed.; D. Lederman, Transl.). Wiley, New York.

SHORTHILL, R. W., MOORE, H. J., SCOTT, R. F., HUTTON, R. E., LIEBES, S., AND SPITZER, C. R. (1976). The "soil" of Mars (Viking I). *Science* **194**, 91–97.

SMITH, D. W., GREENE, T. F., AND SHORTHILL, R. W. (1977). The upper Jovian atmosphere aerosol content determined from a satellite eclipse observation. *Icarus* **30**, 697–729.

SPENGLER, J. D., AND GOKHALE, N. R. (1973). Wake effect interactions of freely suspended large waterdrops. *J. Geophys. Res.* **78**, 497–503.

SRIVASTAVA, R. C. (1971). Size distribution of raindrops generated by their breakup and coalescence. *J. Atmos. Sci.* **28**, 410–415.

STAUFFER, D., AND KIANG, C. S. (1974). Cloud base levels for Jupiter and Venus and the heteromolecular nucleation theory. *Icarus* **21**, 129–146.

STROBEL, D. F. (1975). Aeronomy of the major planets: Photochemistry of ammonia and hydrocarbons. *Rev. Geophys. Space Phys.* **13**, 372–382.

SUTTON, O. G. (1953). *Micrometeorology*. McGraw-Hill, New York.

SUTUGIN, A. G., AND FUCHS, N. A. (1970). Formation of condensation aerosols under rapidly changing environmental conditions. Theory and method of calculation. *Aerosol Sci.* **1**, 287–293.

TENNEKES, H., AND WOODS, J. D. (1973). Coalecence in a weakly turbulent cloud. *Quart. J. Roy. Meteorol. Soc.* **99**, 758–763.

TOON, O. B., AND POLLACK, J. B. (1976). A global average model of atmospheric aerosols for radiative transfer calculations. *J. Appl. Meteor.* **15**, 225–246.

TOON, O. B., POLLACK, J. B., AND SAGAN, C. (1977). Physical properties of the particles composing the Martian dust storm of 1971–72. *Icarus* **30**, 663–696.

TWOMEY, S. (1959a). The nuclei of natural cloud formation. Part I: The chemical diffusion method and its application to atmospheric nuclei. *Geofis. Pura Appl.* **43**, 227–242.

TWOMEY, S. (1959b). The nuclei of natural cloud formation. Part II: The supersaturation in natural clouds and the variation of cloud droplet concentration. *Geofis. Pura Appl.* **43**, 243–249.

*TWOMEY, S. (1977). *Atmospheric Aerosols*. Elsevier, Amsterdam.

VOHRA, K. G., AND NAIR, P. V. N. (1970). Recent thinking on the chemical formation of aerosols in the air by gas phase reactions. *Aerosol Sci.* **1**, 127–133.

VOHRA, K. G., AND NAIR, P. V. N. (1971). Stability of submicron aqueous solution droplets in the atmosphere. *J. Atmos. Sci.* **28**, 280–285.

WALTER, H. (1973). Coagulation and size distribution of condensation aerosols. *Aerosol Sci.* **4**, 1–15.

WARNER, J. (1969). The microstructure of cumulus cloud. Part I. General features of the droplet spectrum. *J. Atmos. Sci.* **26**, 1049–1059.

WATTS, R. G. (1971). Relaxation time and steady evaporation rate of freely falling rain drops. *J. Atmos. Sci.* **28**, 219–225.

WEIDENSCHILLING, S. J., AND LEWIS, J. S. (1973). Atmospheric and cloud structures of the Jovian planets. *Icarus* **20**, 465–476.

WEXLER, R. (1960). Efficiency of natural rain. In *Physics of Precipitation* (H. Weickmann, Ed.), pp. 158–163. Geophys. Monograph No. 5, Amer. Geophys. Union.

WOFSY, S. C., AND SZE, N. D. (1974). Venus cloud models. In *The atmosphere of Venus* (J. E. Hansen, Ed.). NASA SP-382.

WOODS, J. D., AND MASON, B. J. (1964). Experimental determination of collision efficiencies for small water droplets in air. *Quart. J. Roy. Meteorol. Soc.* **90**, 373–381.

YOUNG, A. T. (1973). Are the clouds of Venus sulfuric acid? *Icarus* **18**, 564–582.

YOUNG, A. T. (1975). The clouds of Venus. *J. Atmos. Sci.* **32**, 1125–1132.

YOUNG, A. T. (1977). An improved Venus cloud model. *Icarus* **32**, 1–26.

YOUNG, K. C. (1975). The evolution of drop spectra due to condensation, coalescence and breakup. *J. Atmos. Sci.* **32**, 965–973.